TRW Systems Report
No. 13952-6002-R0-00

PLASMA WAVE MEASUREMENTS FOR THE MARINER TO VENUS AND MERCURY

31 March 1970

National Aeronautics and Space Administration
Contract No. NASW-2041

FINAL REPORT OF THE PLASMA WAVE INSTRUMENT SCIENCE ADVISORY TEAM FOR THE 1973 MERCURY/VENUS MISSION DESIGN

F. L. Scarf	TRW (Team Leader)
R. W. Fredricks	TRW
D. A. Gurnett	University of Iowa
R. E. Holzer	University of California, Los Angeles
S. D. Shawhan	University of Iowa
E. J. Smith	JPL
A. M. Frandsen	JPL (Experiment Representative)

CONTENTS

		Page
I.	SUMMARY STATEMENT	1
II.	SCIENCE OBJECTIVES	3
	II.1 GENERAL MERCURY OBJECTIVES	3
	II.2 WIND-MERCURY INTERACTIONS	3
	II.3 ROLE OF PLASMA WAVES	4
	II.4 PROBLEMS FOR THE 1974 ENCOUNTER	13
	II.5 A STRATEGY FOR ANALYSIS OF THE MERCURY ENCOUNTER	16
	II.6 SECONDARY OBJECTIVES	22
III.	INSTRUMENT CONCEPT	23
	III.1 INTRODUCTION	23
	III.2 BOOM PACKAGE	23
	III.3 SIGNAL PROCESSING AND ELECTRONICS	26
	III.4 INTERFACE REQUIREMENTS	33
	III.5 QUALITY ASSURANCE	35
IV.	EMC CONSIDERATIONS	36
	IV.1 GENERAL SPECIFICATIONS	36
	IV.2 SOLAR PANEL FILTERING	37
V.	TEST PLAN	41
	V.1 SUBSYSTEM AND SYSTEM LEVEL TESTS	41
	V.2 IN-FLIGHT TESTS	45
VI.	REFERENCES	46

CONTENTS

		Page
APPENDIX 1.	MERCURY SURFACE ELECTRICAL PROPERTIES	1.1
APPENDIX 2.	ANOMALOUS RESISTIVITY IN A COLLISIONLESS PLASMA	2.1
APPENXIX 3.	ESTIMATES OF MERCURY'S ATMOSPHERE	3.1

LIST OF ILLUSTRATIONS

		Page
II.1	OGO-5 Bow Shock Observations	6
II.2	Plasma Wave Frequencies from 0.4 to 1 AU	7
II.3	Plasma Conductivity Near Mercury	9
II.4	Unipolar Induction Models	10
II.5	The Venus Interaction (Mariner 5)	12
II.6	The March 30 Dual Occultation Trajectory, and Possible Boundary Crossing	17
II.7	Chorus Emissions (OGO-5); E and Waveform and Spectrum Channel Data	20
III.1	The Electric Field Dipole	24
III.2	OGO Search Coil Sensor	25
III.3	a., b., Sensor Placement on Two Solar Panel MVM '73	27 28
III.4	A General Block Diagram	29
III.5	Low Resolution Spectrum and High Resolution Wave Form E-Field Data (OGO-5) Near Shock	31
1.1	Radar σ of Mercury	1.1
2.1	Current vs Time in a Collisionless Plamsa; Laboratory Measurements of Anomalous Conductivity	2.2

I. SUMMARY STATEMENT

The Plasma Wave Instrument Science Advisory Team has studied the role of a very low frequency (VLF) electric and magnetic wave experiment for the Mariner Venus Mercury '73 mission. The team efforts can be described in terms of three major categories:

a. Development of integrated fields and particles science objectives for the Mercury encounter;

b. Development of cruise science and Venus encounter science objectives and their relationship to the proper interpretation of Mercury encounter observations;

c. Development of a suitable instrument concept for a VLF experiment on a modified Mariner spacecraft.

In these three areas of endeavor, the mutual interaction of the JPL Project Staff, the Science Steering Group, and the Science Instrument Team proved to be of great value. This cooperation resulted in several specific changes in the mission, the spacecraft, and the potential science payload.

Science Objectives at Mercury

In order to analyze the characteristics and evolution of the atmosphere and environment of Mercury it is necessary to understand fully the interaction of the solar wind with the planet. An experiment to measure electric and magnetic wave amplitudes in the frequency range up to 200 kHz gives necessary information on this interaction, and the specific Mercury encounter objectives can be summarized as follows:

a. The plasma wave measurements will provide signatures for the various wind-planet interaction possibilities leading to identification of the interaction type (similar to Venus, Earth, the Moon, or dominated by plasma resistivity).

b. The plasma wave measurements will lead to detailed physical understanding of the microscopic interaction processes that govern the interaction, and affect the atmosphere.

c. The plasma wave experiment will provide very high time resolution support data for other Mariner experiments. This is especially important for the 1973 mission where the planetary encounter is brief.

d. The experiment will detect any wave emissions from Mercury or from low fluxes of charged particles surrounding the planet.

A fully integrated and suitably designed payload will make many decisive tests and yield unambiguous information on the interaction if a dual occultation trajectory is chosen. If the polar flyby trajectory is decided on, then the spacecraft will probably not penetrate the downstream cavity (magnetopause, ionopause, or wake cavity boundary) but detailed measurements of upstream waves and plasma wave turbulence in the sheath can then provide decisive information.

Secondary Objectives

The Mercury interaction study will be strongly supported by measurements in interplanetary space and near Venus. Proper interpretation of the Mercury encounter data requires detailed information about the interplanetary medium near 0.4 AU. Fortunately, MVM'73 will be capable of the high data rate necessary in order to obtain this information. The Venus encounter will provide new information regarding the interaction of the solar wind with planetary atmospheres and will help assure proper interpretation of the Mercury interaction. Thus this single mission can be used to study the interaction of the wind with the Earth and Venus, as well as Mercury, at high data rates permitting detailed comparison of the various planetary encounters.

Instrument Concept

The experiment studied consists of a single-axis search coil ($f \leq 2$ kHz), and a single-axis electric dipole ($f \leq 200$ kHz), along with processing circuits. The final baseline Mariner 1973 spacecraft, with two solar panels, moderate panel noise filtering and simple experiment booms, provides an excellent platform for a plasma wave experiment.

Instrumentation concepts examined during the study period involve bandwidth maximization, quality assurance specifications, and definition of a "minimum" instrument. A minimum cost instrument (based on use of previously-flown hardware, deletion of some on-board processing channels, and reliance on OGO-type quality assurance specifications) can be used to obtain much of the necessary information. If a significant portion of the nominal baseline telemetry rate of 16 kilobits/sec is available, unique audio-frequency waveform data will be obtained with this minimum instrument. These direct transmissions of high rate waveform data from Mercury, Venus, and the inner solar wind can be used to perform detailed spectral analysis on the ground. The scientific return is then maximized, but this simplified experiment places relatively little burden on the spacecraft.

II. SCIENCE OBJECTIVES

II.1 GENERAL MERCURY OBJECTIVES

The solar wind flows steadily past Mercury, and it interacts strongly with the planetary atmosphere, the magnetic field, the plasma sheath, or the surface. Mercury also must strongly perturb the wind, but the interplanetary plasma is very dilute, even at 0.4 AU, and these perturbations have to involve collective processes (plasma waves) rather than particle-particle collisions. In order to analyze the characteristics and evolution of the atmosphere and environment of Mercury it is necessary to understand fully the interaction of the solar wind with the planet, including the excitation processes for these local waves. The plasma wave measurements also provide unique identification of the interaction type, and this capability is especially vital for the single high speed flyby mission under consideration for 1973-1974.

In the following sections we describe briefly the possible wind-Mercury interactions, discuss the physical roles played by plasma waves, enumerate some observational problems that are particularly relevant for the 1973 Mariner Mission, and outline a coordinated strategy for the exploration of Mercury.

II.2 WIND-MERCURY INTERACTIONS

The interface regions between the solar wind and the Earth, Moon, Venus and Mars have been explored during the last decade, and it is possible to classify the interactions into at least three very distinct types corresponding to encounter with different obstacles:

A. Magnetopause (Earth). The planetary magnetic field is compressed on the day side and drawn out into a very long extended tail in the antisolar direction. A detached bow shock forms with r(shock) $\simeq$ 1.4 r(boundary). For the earth r(boundary) $\simeq$ 10 R_e at local noon, and energetic particles are trapped within the magnetosphere. If Mercury has a sufficiently large magnetic field ($M \gtrsim 10^{-4}\ M_e$) then the predicted magnetopause will be above the surface and the atmosphere will be protected from the wind.

B. Ionopause (Venus, Mars). For planets having relatively dense atmospheres but without intrinsic magnetic fields of sufficient strength to deflect the wind, the solar wind must impinge on the top of the planetary atmosphere. If the neutral pressure is sufficient to stop the wind above the surface [$p(\text{wind}) = NmU^2 \simeq 10^{-10}$ mb for $N = 33$ cm^{-3}, $U = 400$ km/sec], then a photochemical ionosphere results. In this case the plasma is conducting enough so that the interplanetary field builds up and stands off the wind, again producing a detached bow shock (Cloutier, McElroy and Michel, 1969).

C. Surface (Moon). If the non-magnetic obstacle has a very dilute neutral atmosphere, then ions are rapidly swept to the surface, preventing formation of a durable ionosphere. If the equivalent electrical conductivity of the planet is sufficiently low ($\sigma \lesssim 10^{-5}$/ohm meter for the Moon), then the interplanetary field freely passes into and past the obstacle, so that no strong detached bow shock forms (a weak limit shock cannot be ruled out). A plasma wake cavity exists behind the obstacle.

Our present knowledge of Mercury and its environment is very incomplete, and some other possible interactions cannot be excluded. If the effective bulk planet conductivity is high, then the time constant,

$$\tau = \frac{4\sigma\mu L^2}{\pi c^2}$$

for decay of magnetic field in a sphere of radius L (gaussian units) is long, and the interplanetary field cannot penetrate the planet. For the lunar case (as noted above), any $\sigma \gtrsim 10^{-5}$ (ohm-m)$^{-1}$ (MKS units) would "hang up" the field and cause a shock; the absence of a clear lunar bow shock therefore suggests $\sigma \lesssim 10^{-5}$/ohm meter. However, in the case of Mercury, we now know only that $\sigma \lesssim 2 \times 10^{-2}$ (ohm-meter)$^{-1}$ (Appendix 1). Thus, we cannot now rule out a conducting-planet model in which the core would produce a magnetic obstacle for the wind. In this case unipolar induction phenomena would generate heat in the core (Colburn et al., 1967), and the net dissipation would be critically dependent on the return currents that develop in the planetary sheath region. The anomalous conductivity associated with wave-particle scattering (next section) would then govern the transfer of heat to the core.

II.3 THE ROLE OF PLASMA WAVES IN THE WIND-MERCURY INTERACTION

In general, individual charged particles may be deflected because they interact with other single particles (binary coulomb collisions), with static electromagnetic fields, or with groups of charged particles that are organized to produce plasma waves. However, the wind is very dilute even at Mercury and coulomb collisions cannot play a very significant role in the planetary encounter. As discussed in II.2, the planet environment may be dominated by an intrinsic or induced magnetic field that deflects particles or by an induced unipolar electric field that allows them to flow toward the surface, but in every case, the interactions of solar wind particles with local plasma turbulence (waves) must provide an important source of energy and momentum transfer and a clear signature of the interaction type.

If any kind of detached bow shock forms, then a collisionless dissipation mechanism involving wave excitation is responsible because the proton collision mean free paths at 0.4 AU are enormous. Several wave-particle dissipation mechanisms have recently been examined experimentally for the Earth's bow shock, and Figure II.1 shows an OGO-5 example. The shock encounter at about $0^h52^m32^s$ UT is marked by rapid changes in proton temperature, velocity and flow direction (Lockheed and JPL plasma data), and by enhanced electrostatic ion acoustic noise (TRW E-field) as well as by enhanced electromagnetic whistler mode noise (JPL/UCLA dB/dt levels).

The microscopic wave-particle interaction leading to rapid thermalization can be described in terms of the anomalous electric conductivity that develops in a collisionless plasma. Whenever the electric currents become large enough so that the relative particle streaming speed exceeds the wave phase speed, waves are generated and they then scatter the particles. The current is limited by this scattering, and $j \lesssim \sigma E$ with

$$\sigma = \frac{Ne^2}{m\nu_{eff}}$$

where ν_{eff} is related to the wave frequency. This concept is discussed further in Appendix 2, and it is noted that $\nu_{eff} \simeq 0.1\ \omega_{p+}$ is roughly appropriate if the scattering comes from ion sound waves, and $\nu \simeq 0.35\ \omega_{p+}$ if large amplitude Buneman modes provide the plasma turbulence. These estimates appear to be appropriate for laboratory shocks (Paul et al., 1969; Bratenahl and Yeates, 1970) and for the Earth's bow shock (Fredricks et al., 1970).

We now know very little about the microstructure of the solar wind within about 0.6 AU, and these uncertainties make it impossible to describe the wave-particle interactions near Mercury with complete assurrance. However, it is possible to use the Parker model to interpolate between 1 AU and the corona in order to identify the important wave frequencies that depend only on local density and magnetic field strength. Figure II.2 shows how the ion and electron plasma frequencies $[(f_p)_\pm = \omega_{p\pm}/2\pi]$ and cyclotron frequencies $[(f_c)_\pm = \omega_{c\pm}/2\pi]$ vary with distance toward 0.4 AU (this graph also shows why a 2 kHz range for the magnetic sensor is adequate $[f_{c-}\ (0.4\ AU) \lesssim 2\ kHz]$ while a much broader range is desirable for E $[f_{p-}\ (0.4\ AU) \lesssim 200\ kHz]$).

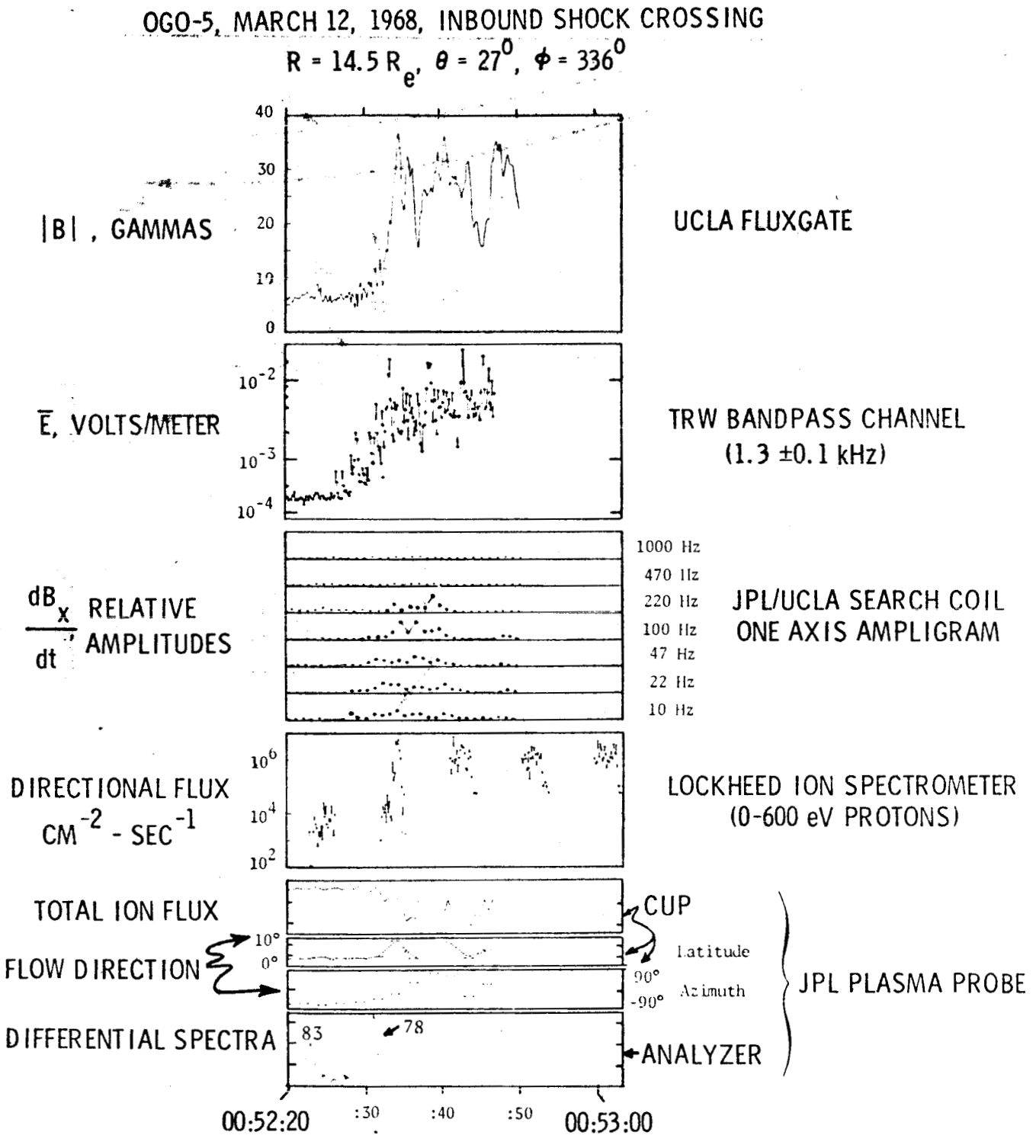
OGO-5, MARCH 12, 1968, INBOUND SHOCK CROSSING
R = 14.5 Re, θ = 27°, φ = 336°
|B| , GAMMAS
40
30
20
10
0
UCLA FLUXGATE
E, VOLTS/METER
10-2
10-3
10-4
TRW BANDPASS CHANNEL
(1.3 ±0.1 kHz)
dBx/dt RELATIVE AMPLITUDES
1000 Hz
470 Hz
220 Hz
100 Hz
47 Hz
22 Hz
10 Hz
JPL/UCLA SEARCH COIL
ONE AXIS AMPLIGRAM
DIRECTIONAL FLUX
CM-2 - SEC-1
10^6
10^4
10^2
LOCKHEED ION SPECTROMETER
(0-600 eV PROTONS)
TOTAL ION FLUX
CUP
FLOW DIRECTION
10°
0°
Latitude
90°
-90°
Azimuth
DIFFERENTIAL SPECTRA
83
78
ANALYZER
JPL PLASMA PROBE
00:52:20
:30
:40
:50
00:53:00

Figure II.1

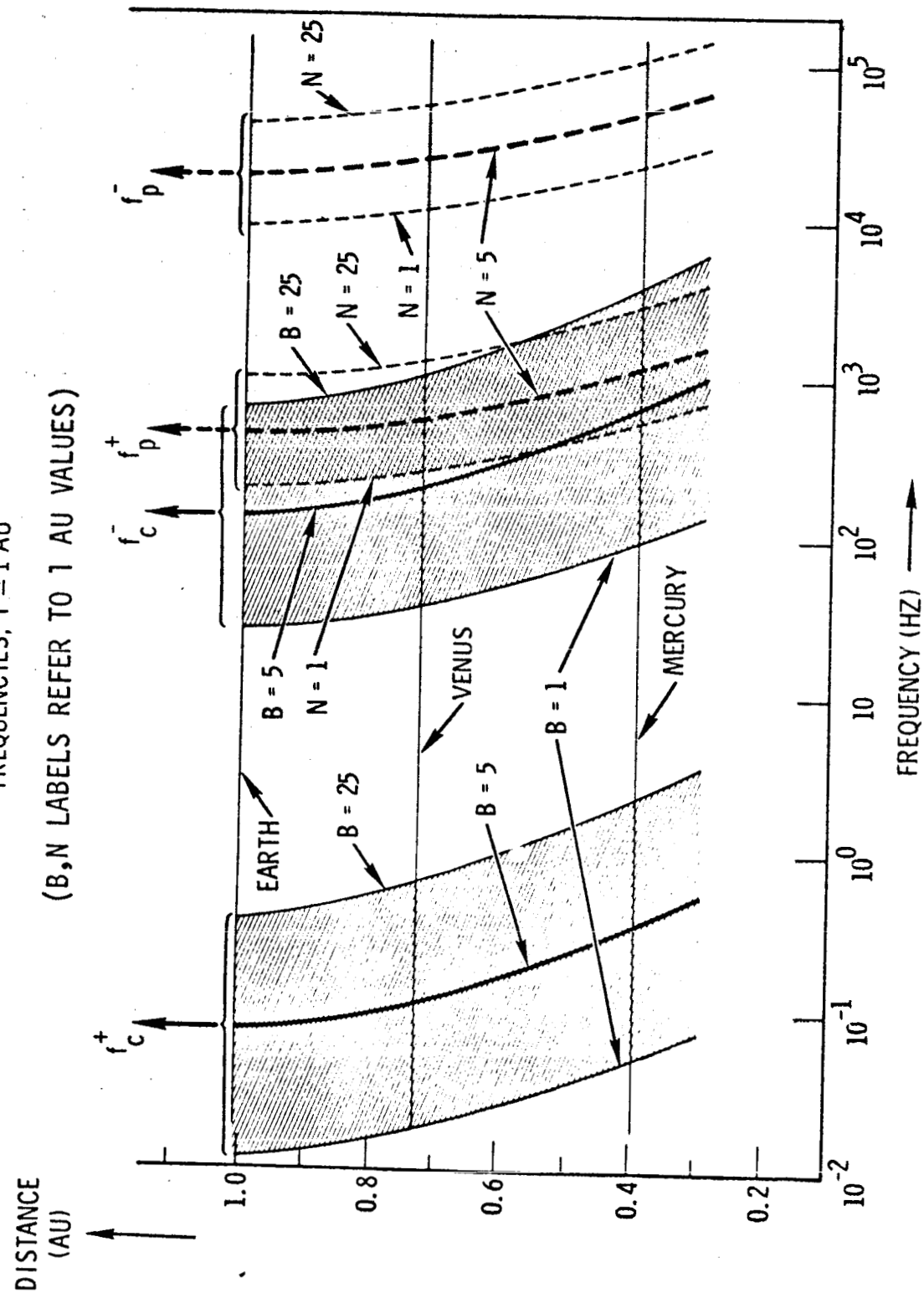
CHARACTERISTIC PLASMA WAVE
FREQUENCIES, r ≤ 1 AU
(B,N LABELS REFER TO 1 AU VALUES)
DISTANCE
(AU)
1.0
0.8
0.6
0.4
0.2
EARTH
VENUS
MERCURY
B = 25
B = 5
B = 1
N = 1
N = 25
f_c^+
f_c^-
f_p^+
f_p^-
10^{-2}
10^{-1}
10^0
10
10^2
10^3
10^4
10^5
FREQUENCY (HZ)

Figure II.2

The anomalous plasma conductivity depends only on wave frequency, and therefore in the case of ion sound waves [excited with a drift speed greater than $(\kappa T_e/m_i)^{1/2}$] or Buneman modes [excited with drift speed greater than $(\kappa T_e/m_e)^{1/2}$] only the plasma density enters. Figure II.3 shows a conductivity versus current density profile computed for the solar wind plasma in the neighborhood of Mercury. For $j \lesssim 5 \times 10^{-11}$ amp/cm^2, the plasma should be relatively stable and the very high coulomb conductivity should apply, leading to use of the conventional mhd description. For $5 \times 10^{-11} \lesssim j \lesssim 2 \times 10^{-9}$ amp/cm^2, ion sound waves should be strongly excited (see Appendix 2) with $\sigma_{eff} \sim 10^{-3}$ (ohm-meter)$^{-1}$ and for higher drift speeds, large amplitude Buneman modes should lead to a further reduction in plasma conductivity.

In Appendix 1 it is shown that radar observations now give an upper bound for Mercury's surface conductivity of 2×10^{-2} (ohm-meter)$^{-1}$. The actual surface conductivity of Mercury can be much smaller than this bound, and it may certainly be as low as the apparent lunar value, $\sigma_{(Moon)} \lesssim 10^{-5}$ (ohm-meter)$^{-1}$. The fact is that radar determinations are not very sensitive, and the most accurate bound on the effective lunar bulk conductivity comes from study of particles and fields data near the Moon. This kind of intimate relation between the planetary electrical and magnetic properties and the plasma environment must also extend to Mercury, as discussed in Section II.2.

However, Figure II.3 shows that we cannot completely exclude the possibility that the unstable plasma surrounding Mercury is a poorer conductor than the planetary surface. This means that a fourth general type of planet-wind interaction must be considered, and Figure II.4 compares some aspects of a "conducting surface" model with the lunar-type "insulating surface" model. The top panel in Figure II.4 shows the basic circuit diagram for the unipolar system that can be appropriate when the intrinsic planetary magnetic field and atmosphere are too weak to produce significant wind deflections. The upstream solar wind has $(\underset{\sim}{E} + \underset{\sim}{v} \times \underset{\sim}{B}) \simeq 0$, and finite conductivity effects are never meaningful in the unperturbed plasma. If the illuminated sheath-limb shock region is also relatively ordered and quiet, then this region represents a good conductor for return currents, and the poorest conductor in the circuit is the planet (Moon) itself. In this case the only relevant parameter is the effective bulk conductivity of the planet. For the lunar case $\sigma < 10^{-5}$ (ohm-meter) allows field diffusion leading to the void shown in the central panel of Figure II.4, while $\sigma > 10^{-5}$ gives some field build-up, perhaps leading to a detached bow shock similar to the Venus-Mars case.

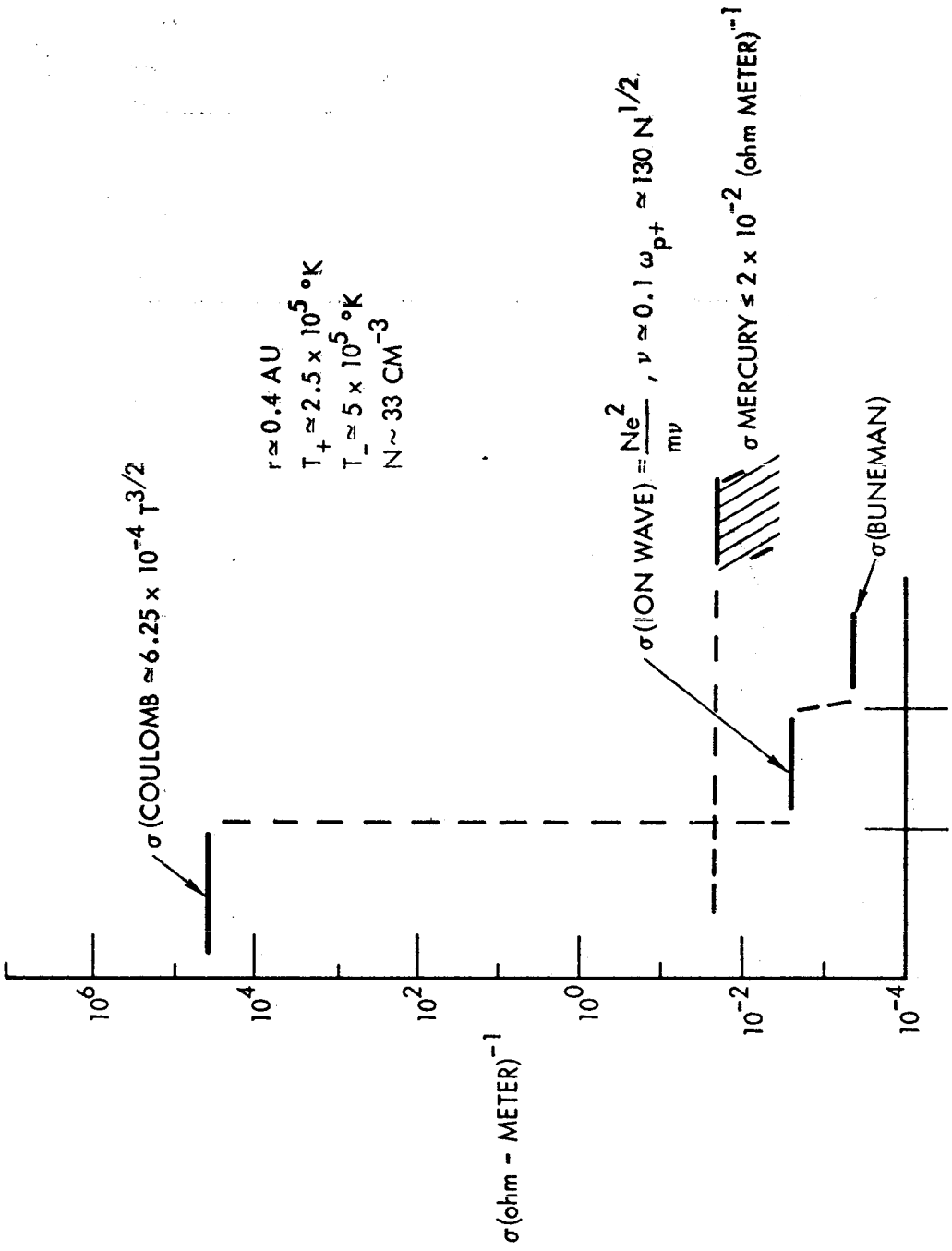
σ (COULOMB ≃ 6.25 × 10⁻⁴ T^3/2
r ≃ 0.4 AU
T+ ≃ 2.5 × 10^5 °K
T− ≃ 5 × 10^5 °K
N ~ 33 CM^-3
σ (ION WAVE) = Ne²/mν , ν ≃ 0.1 ω_p+ ≃ 130 N^1/2
σ MERCURY ≤ 2 × 10^-2 (ohm METER)^-1
σ (BUNEMAN)
σ (ohm - METER)^-1
10^6
10^4
10^2
10^0
10^-2
10^-4
5 × 10^-11
2 × 10^-9
CURRENT DENSITY (AMP/CM^2)

Figure II.3

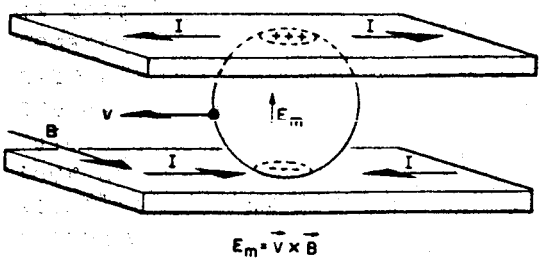

Idealized model of the unipolar generator for the spherical geometry of a planet and the solar wind.

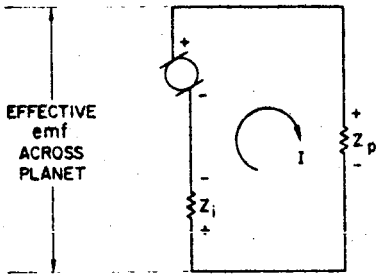

Conceptual circuit representing the path of the currents for the unipolar system. The two impedances are the mean internal impedance, Z_i, and the outer or plasma impedance, Z_p. The generator is the motional potential difference across the body.

(SONETT AND COLBURN, 1968)

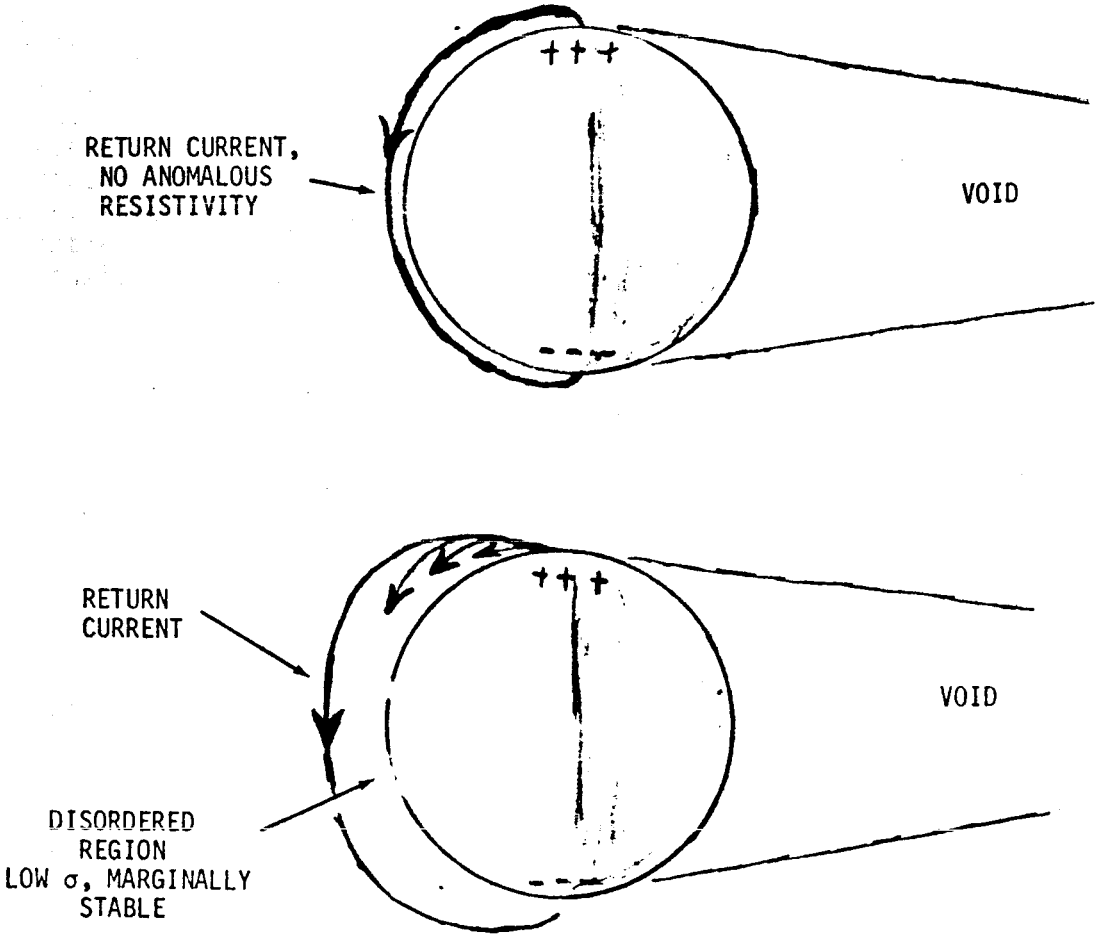

Figure II.4

The novel possibility for Mercury, suggested by Figure II.3, is that Z_p, the plasma impedance, will be higher than the internal impedance Z_i. The consequences for this type of interaction have not been examined in great detail, but the lowest panel in Figure II.4 illustrates one aspect of this situation. If Z_p is governed by current-driven anomalous conductivity effects, the return currents would seek a path further upstream, reducing the local current density so that the plasma instabilities would tend to marginal stability. In this case a disordered region with low σ would tend to spread outward on the front hemisphere and extremely large amplitude plasma waves would develop to scatter the incoming wind particles.

The understanding of the solar wind-planet interaction is fundamental if we wish to achieve understanding of the temporal development and present state of Mercury's atmosphere and ionosphere. The nominal solar wind pressure at 0.4 AU is about 10^{-10} millibars ($N = 33/cm^3$, $u = 400$ km/sec, NkT, $B^2/8\pi \ll Nmu^2$) and this is small compared to the anticipated atmospheric pressure; reports of the UV Science Advisory Team for MVM '73 cite an upper limit of 2-10 mb and preferred theoretical predictions of 10^{-6} - 10^{-8} millibars for the atmospheric pressure. Nevertheless, if the solar wind does flow into the atmosphere, the streaming magnetized plasma will provide a major loss mechanism for certain atmospheric constitutents. A sample calculation for a model Mercury atmosphere is contained in Appendix 3. It is shown, for example, that the solar wind scouring (scattering) of atmospheric gases in the limb regions produces an important loss mechanism. Charge exchange and $\underset{\sim}{v} \times \underset{\sim}{B}$ "pickup" are also obviously very significant.

Since all of these loss mechanisms are selective, it is clearly necessary to understand in detail the extent to which the atmosphere is protected from the solar wind. In fact, the wave-particle interaction phenomena discussed above can provide extremely important atmospheric energy and momentum transfer mechanisms. These must be identified and analyzed in order to interpret correctly the planet encounter data.

One likely example of an important collisionless interaction is found in the Mariner 5 Venus encounter data. Figure II.5 shows the magnetometer and plasma probe observations, along with the rotated encounter trajectory, and we note the prominent enhancement in N (top panel) and in $|\underset{\sim}{B}|$ (center) between points 4 and 5. These enhancements are not predicted by the aerodynamic flow calculations, and G. Siscoe has suggested the explanation outlined on the lower right-hand side of Figure II.5; if cool ionospheric electrons exchange with warm wind electrons, then the electron contribution to the incident pressure balance is effectively removed. This requires an increase in B,N and it implies that thermal energy flows directly into the Venus ionosphere, while the wind in the sheath is locally cooled by the presence of ionosphere electrons.

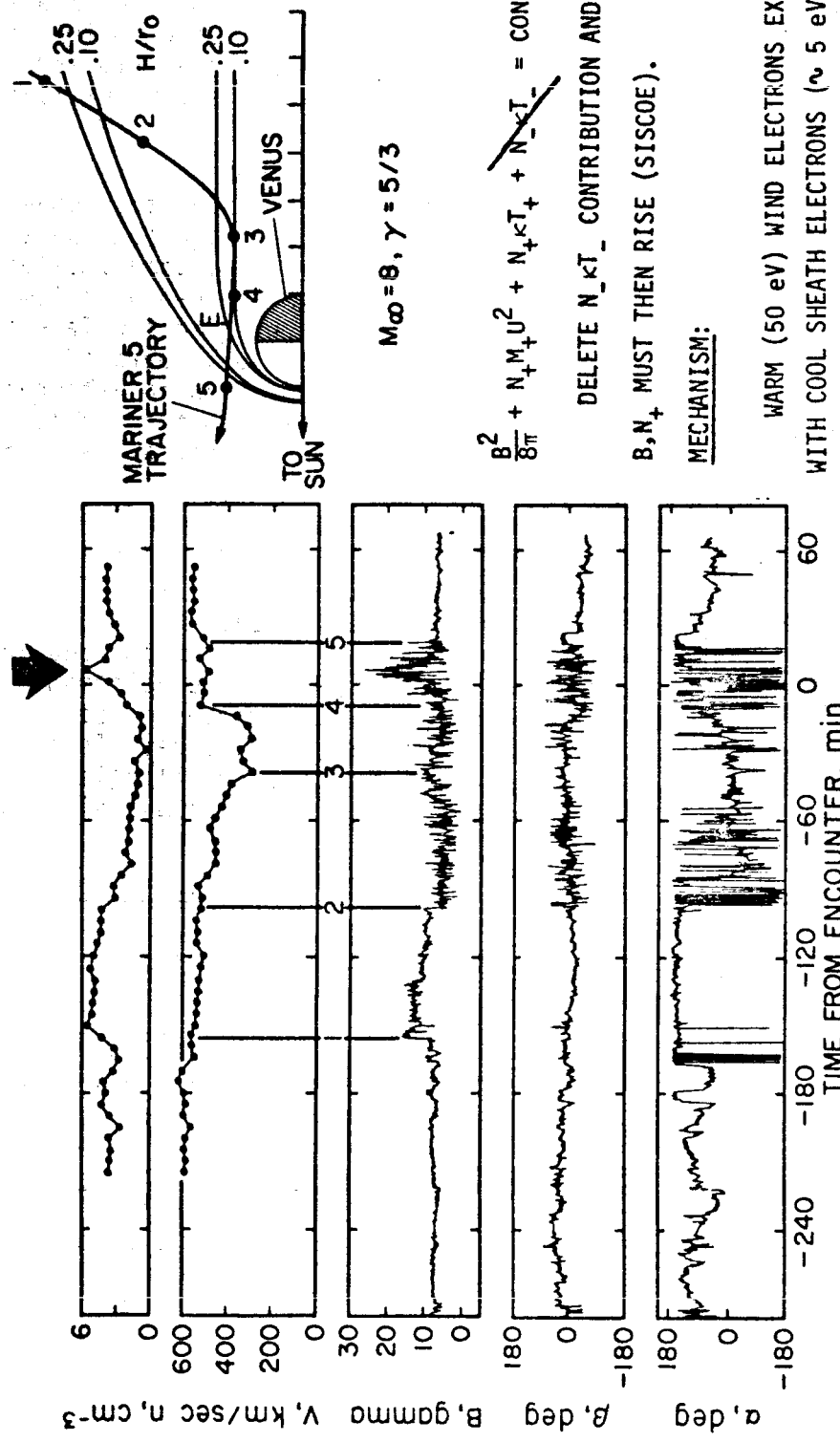
MARINER 5 TRAJECTORY
TO SUN
VENUS
H/r₀
.25
.10
.25
.10
M∞=8, γ=5/3
$\frac{B^2}{8\pi} + N_+M_+U^2 + N_+\kappa T_+ + N_-\kappa T_- = \text{CONST.}$
DELETE $N_-\kappa T_-$ CONTRIBUTION AND
B,N_+ MUST THEN RISE (SISCOE).
MECHANISM:
WARM (50 eV) WIND ELECTRONS EXCHANGE WITH COOL SHEATH ELECTRONS (~ 5 eV) OR COLD IONOSPHERE ELECTRONS (< 1 eV), EFFECTIVELY REMOVING $N_-\kappa T_-$.
ONLY ENERGY IS TRANSFERRED BY THIS "HEAT CONDUCTION" INTERACTION.
α, deg
β, deg
B, gamma
V, km/sec
n, cm⁻³
TIME FROM ENCOUNTER, min

Figure II.5

This explanation requires plasma turbulence to provide short scattering lengths since the electron coulomb mean free path is much too long to allow the indicated exchange. A natural source for this turbulence is the two-stream plasma instability that should develop when the wind or sheath plasma flows directly into the Venus ionosphere (Scarf, 1963), and a similar process could well develop on Mercury. In this case the plasma waves play a direct role in determining the energy balance, location, and profile of the ionosphere.

More complex interactions of this type are also possible if Mercury has no protective magnetic field. Wave-particle interactions can cause exchange of solar wind protons with planetary positive ions (argon, helium, etc.). These direct exchanges would produce temporary unstable (multi-humped) distributions that would provide rapid wave growth, until the slow ions were sufficiently accelerated and thermalized. In contrast to the case of electron exchange, any such positive ion exchange involves transfer of energy and momentum. Thus, the interaction associated with scattering from plasma turbulence would give rise to an effective heat flow and a viscous drag.

II.4 PROBLEMS FOR THE 1974 ENCOUNTER

Successful planning for the initial exploration of any planet or uncharted region of space must take into account previously acquired information of relevance. In addition, all known problems and uncertainties have to be recognized, and others must be anticipated. Analysis of the potential mission profile for the Mariner-Venus-Mercury flyby shows that some very significant tactical problems are present, and these must play a large role in the design of the experiments and choice of the encounter trajectory.

Lack of Knowledge of Mercury

The first Mariner flights to Mars and Venus were designed without knowledge of the planetary magnetic field or magnetosphere, but ground-based observations showed that each planet did have a significant atmosphere. The Pioneer-Jupiter missions were also able to be designed with fairly certain knowledge that a magnetosphere and associated shock would be encountered. By contrast, we now have available no corresponding guide to plan for in situ study of the Mercury environment. The high density of Mercury could mean that a sufficiently strong intrinsic planetary magnetic field exists, but the slow rotation rate can be used to argue against this conjecture. Present estimates of the Mercury atmospheric pressure vary over more than 10 orders of magnitude, and these estimates do not offer useful guidelines. The radar bound on the Mercury surface conductivity (Appendix 1) is also so high that many models can be accomodated, as described in Sections II.2, II.3. Thus, the mission plans must consider an unusually large number of possible environmental situations.

Uniqueness of the 1974 Encounter

The Venus swingby opportunity is rare, and there are now no plans for additional direct flights to Mercury. Thus, the payload selection for the 1973-74 Mariner Mission will have special importance. Since this may be the only Mercury flight for a great many years, the experiments have to provide complete and unambiguous information on all aspects of the planet encounter.

Lack of Knowledge of the Inner Solar Wind

The solar wind parameters describing the bulk flow characteristics can readily be computed for 0.4 AU. The top four lines in Table 1 give representative values for density, streaming speed, field strength, and dynamic pressures at 0.4 and 1 AU, and these straightforward extrapolations are simply based on the Parker model. However, in a very real sense we now know essentially nothing about the solar wind microstructure at 0.4 AU, and the bottom seven lines in Table 1 contain some brief summary statements about these uncertainties. The solar wind distribution functions observed near 1 AU are non-Maxwellian in a number of important ways [e.g., $T_- > T_+$, $T_{\parallel} > T_{\perp}$; there is a large third moment; suprathermal protons and electrons appear sporadically], and the evolution of the distribution observed near Earth is not understood. However, it is known that the wind at 1 AU is an unstable collisionless plasma, and that some interplanetary wave-particle interactions have already operated to produce the observed distributions.

This lack of knowledge is very significant with respect to the 1973 Mercury mission for a number of reasons. As described above, the wind-planet interactions involve plasma turbulence, but the form of wave excitation depends on those details of the microstructure that are least understood. Moreover, at present we do know the characteristic signatures of various interplanetary features (shocks, tangential discontinuities, M-regions, etc.) near 0.4 AU, yet a full understanding of Mercury's role as a solar wind target requires complete understanding of the incident beam parameters, and knowledge of the way to distinguish between interplanetary and planetary disturbances.

Encounter Speed

The arrival speed at Mercury is unusually high for a planetary encounter. Figure II.6 shows a possible dual occultation trajectory, and the minimum shock and cavity boundaries are roughly sketched. One-minute marks are indicated on the spacecraft trajectory, and it can be seen that the total encounter time from shock crossing to shock crossing may be as small as 25 minutes. The time in the cavity can be less than 10 minutes. To appreciate how brief the encounter is, we note the following:

QUANTITY	1 AU	0.4 AU	REMARKS
DENSITY	5 cm^{-3}	33 cm^{-3}	
VELOCITY	400 km/sec	400 km/sec	
B-FIELD	5γ	25γ	
PRESSURE	1.5×10^{-11} mb	9×10^{-11} mb	
$\langle T_+ \rangle$	7×10^4 °K	?	DENSITY FIT GIVES $\gamma \sim 3/2$; COLLISIONLESS PROCESSES CAN DETERMINE T VARIATION
$\langle T_- \rangle$	2×10^5 °K	?	OBSERVED (T_+/T_-) RATIO AT 1 AU MIGHT BE EXPLAINABLE BY TWO-FLUID MODEL, BUT ADDITIONAL e-p ENERGY TRANSFER MAY OCCUR
PROTON ANISOTROPY ($T_{\parallel}/T_{\perp}$)	~ 3	?	OBSERVED SMALL ANISOTROPY AT 1 AU SUGGESTS WAVE-PARTICLE INTERACTIONS WELL WITHIN ONE AU.
ELECTRON ANISOTROPY	~ 1.1	?	SAME AS ABOVE
NON-THERMAL PARTICLES	FIELD ALIGNED HIGH ENERGY TAIL USUALLY PRESENT	?	PARTICLES AT 1 AU ARE OBSERVED TO LOSE ENERGY RAPIDLY. THEY MAY BE LOCALLY ACCELERATED, OR FLOW FROM SUN. THEY SHOULD BE VERY IMPORTANT CLOSER TO SUN.
HEAT CONDUCTION	$\sim 10^{-2}$ ergs/cm^2sec	?	HEAT FLUX INSTABILITIES ARE POTENTIALLY VERY IMPORTANT WELL WITHIN 1 AU.
WAVES PRODUCING SHOCK DISSIPATION	ALFVEN WAVES ION SOUND WAVES WHISTLERS	?	THE WIND AT 0.4 AU IS COLLISIONLESS. SOME KIND OF WAVE EXCITATION IS NEEDED TO SUPPORT A DETACHED BOW SHOCK OR A LIMB SHOCK

Table 1

a. On Mariner 5, the time between initial and final shock crossings was about three hours, as shown in Figure II.5.

b. If a 4°/sec scan platform with 120° angular range is to be used for the plasma probe, then complete characteristics of the streaming plasma will be measured once every 30 seconds. For the trajectory of Figure II.6, this gives about 32 complete scans before earth occultation, and 15-20 scans across the entire cavity.

c. The bow shock observed near Earth has a thickness, δ, roughly equal to c/ω_{p-} (see Figure II.1). For $N = 33\ cm^{-3}$, $f_{p-} = \omega_{p-}/2\pi \simeq 52$ kHz and δ(Mercury) then scales to about 900 meters. With a 10 km/sec encounter speed this shock could be traversed in about 90 milliseconds, as indicated. A very important measurement is the strength of the shock, since a weak limb shock might be present even if a lunar type interaction occurs. Multiple shock crossings are also commonplace, and these considerations reflect the need for very high time resolution diagnostics.

Gross Similarity of Various Situations

As shown in Figure II.6 all models lead to some sort of plasma cavity behind Mercury, and for any traversal near the dawn-dusk meridian, a weak limb shock might be found in nearly the same place as a strong detached bow shock. Aberration effects and non-radial flow can also move these boundaries around, and the boundary locations will probably not be reliable guides to the interaction type.

II.5 A STRATEGY FOR ANALYSIS OF THE MERCURY ENCOUNTER

Some of the problems discussed above can be alleviated in simple ways. For instance, moderately extensive monitoring of the solar wind within about 0.6 AU, with science telemetry rates similar to those planned for encounter, will help in distinguishing interplanetary and planetary disturbance features.

Another very relevant decision involves choice of the Mercury encounter trajectory. During the SSG planning phase, three trajectories were selected for detailed study: March 30, $\theta = 20°$ (earth and sun occultation), April 1, $\theta = 80°$ (earth occultation only), and April 1, $\theta = 105°$ (no occultation). All of these should penetrate a strong bow shock and be able to measure some important characteristics of upstream waves and sheath flow. However, the April 1, 105° orbit is least favored because it will not penetrate the cavity, and since there is no Earth occultation, no day-side density profile can be deduced from the Radio Science experiment.

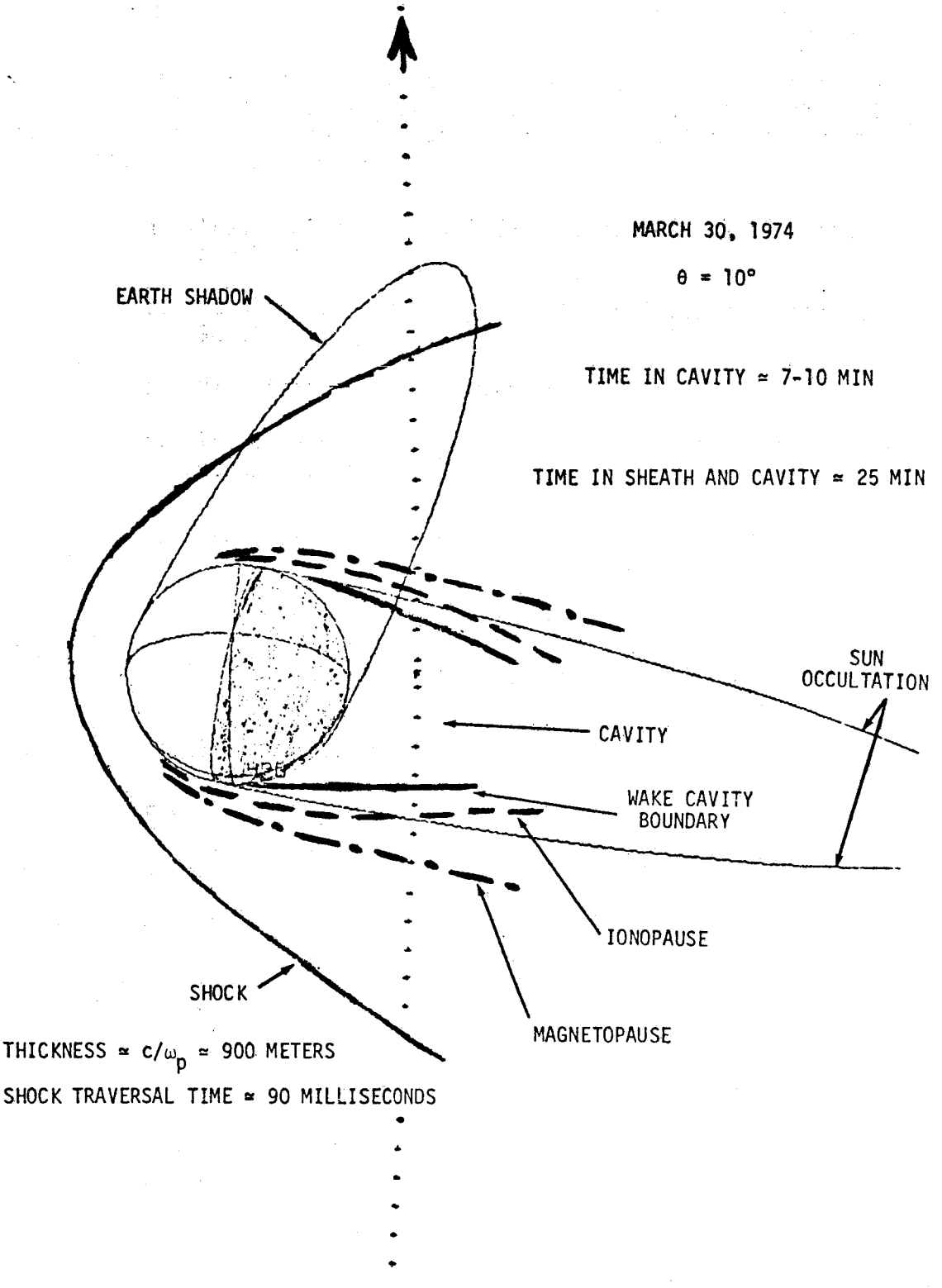
MARCH 30, 1974
θ = 10°
TIME IN CAVITY ≃ 7-10 MIN
TIME IN SHEATH AND CAVITY ≃ 25 MIN
EARTH SHADOW
SUN OCCULTATION
CAVITY
WAKE CAVITY BOUNDARY
IONOPAUSE
SHOCK
MAGNETOPAUSE
THICKNESS ≃ c/ω_p ≃ 900 METERS
SHOCK TRAVERSAL TIME ≃ 90 MILLISECONDS

Figure II.6

The April 1, $\theta = 80°$ profile is better on these two counts, but the Plasma Wave Team concludes that a March 30, $\theta = 20°$ pass offers the best scientific potential for the exploration of Mercury and its environment. This dual occultation pass would provide:

a. Traversal of the maximum number of characteristic boundaries.

b. Supplementary dayside density profiles from the Radio Science Experiment.

c. Maximization of time within the sheath.

d. The opportunity to explore directly within the downstream cavity.

However, even for the dual occultation trajectory, severe interpretive problems remain when the encounter is examined from the point of view of a single experiment. The correct strategy for this flyby mission to an unexplored planet in an unknown plasma environment must involve development of a coordinated and integrated set of measurements from several compatible experiments. It is unlikely that any one experiment will make completely decisive measurements, but when the results from several diagnostics are examined, the overall pattern should be consistent with only one model of the Mercury environment.

For this approach to be successful we must identify many decisive individual measurements and design the experiments accordingly. Some examples of simple measurements of this type are worth noting:

a. If the magnetic field in the cavity has a distinctly different direction than the one in the sheath or interplanetary space, we may conclude with a high degree of confidence that some planetary magnetic field is detected here. The lunar type interaction is then ruled out, but the planetary field may still be intrinsic or induced in the ionosphere. Thus, this measurement alone does not completely determine the interaction.

b. If the low frequency ($f \lesssim f_{ce}$) power spectrum in the cavity falls regularly with increasing frequency, then we are probably examining some modified interplanetary field, or temporary (induced) planetary field. However, if the E and B power spectrum is peaked at $f_{ce}/4 \lesssim f \lesssim f_{ce}/2$, then our experience

in the Earth's magnetosphere would suggest a chorus-like noise source. This indicates that low energy trapped or quasi-trapped particles are present suggesting an intrinsic planetary field. In fact, the inference is reasonable even if the particle fluxes are too low to be measured directly by on-board instruments.

The detection of chorus spectra or other electrostatic emissions from Mercury would be extremely significant because knowledge that particles are trapped gives non-local information on the magnetic field configuration. If these electromagnetic waves are detected and identified, then it is also possible to evaluate the local plasma density. Figure II.7 shows some OGO-5 chorus E and B data (waveform on left, spectrum on right), and in the bottom section it is shown that the measured E, B amplitudes do provide an excellent density determination.

c. If cold electrons are detected at the cavity boundary, then the ionopause model is probably appropriate (see Figure II.5 and related discussion). However, if hot electrons are detected at the boundary, then the model with anomalous plasma resistivity is most likely.

No one of these possibilities leads to completely unambiguous identification of the Mercury interaction and environment, but since these individual measurements contribute greatly to the overall picture, it is clear that a) the magnetometer should have direction-measuring capability; b) the plasma wave experiment should provide E and B coverage over the chorus range; c) the plasma probe should have electron channels.

Many other decisive measurements must be made. We attempt to summarize briefly some specific measurements and their implications in Table 2. This partial checklist shows that a single result is frequently compatible with a number of models. However, when enough measurements of significance are made the overall pattern unambiguously points to one sequence of events or another.

In conclusion, we feel that the problems discussed in Section II.4 can only be treated by this type of coordinated approach, and we recommend that the final payload should contain an integrated set of experiments specifically designed for the brief Mercury encounter.

OGO-5, AUGUST 15, 1968

f_{ce} = 2.2 khz, L = 6.4, 0104 LOCAL TIME, $\lambda_m = -2^0$

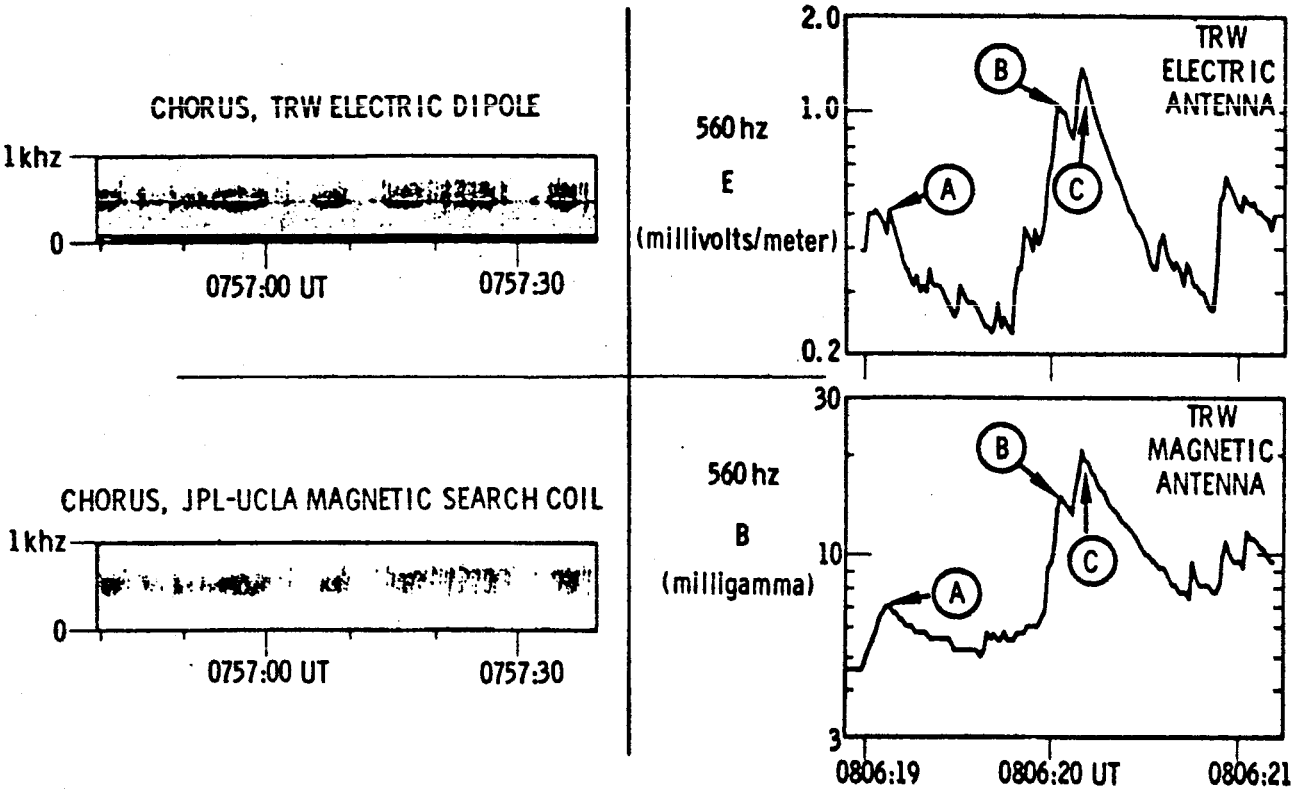

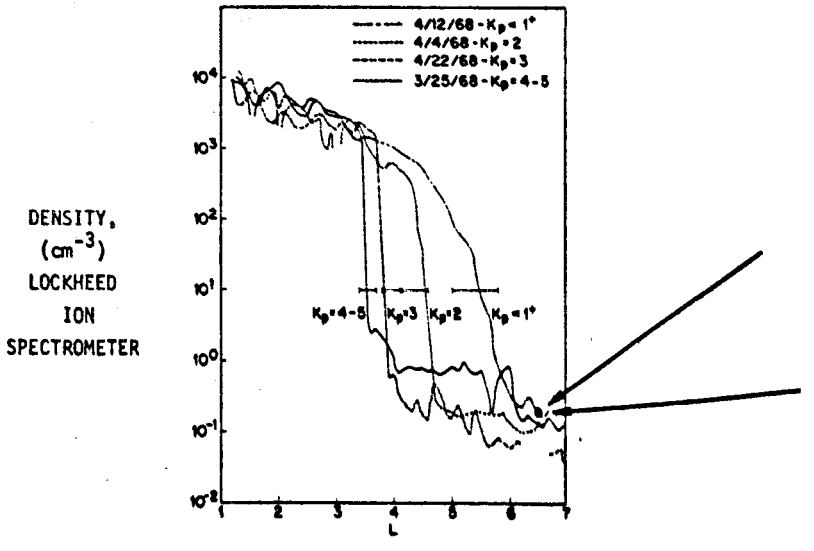

N = 0.2 - 0.3 cm^{-3}, MEASURED DIRECTLY BY LOCKHEED SPECTROMETER ON AUGUST 15, 1968 AT 0800 UT (K_p = 4)

N = 0.2 cm^{-3}, DEDUCED USING

$$\frac{c^2E^2}{B^2} = 1 + \frac{f_p^2}{f(f_c - f)}$$

WITH MEASURED 560 HZ E AND B CHORUS AMPLITUDES AT 0800 UT, AUGUST 15, 1968

Figure II.7

	MAGNETOSPHERE	IONOSPHERE	CONDUCTING SURFACE	WIND HITS SURFACE
STRONG SHOCK EXISTS	X	X	X	
LAMINAR FLOW IN SHEATH	X	X		
TURBULENT FLOW IN SHEATH			X	
$f < f_{ce}$ NOISE IN CAVITY	X			
INTENSE ION WAVES THROUGHOUT SHEATH			X	
INTERPLANETARY FIELD IN CAVITY				X
ELECTRON PLASMA OSCILLATIONS AT CAVITY BOUNDARY		X		
HOT ELECTRON LAYER AT CAVITY BOUNDARY			X	
COLD ELECTRONS AT BOUNDARY; INCREASE IN N,B		X		X
CAVITY RADIUS SMALLER THAN PLANET		X(?)	X(?)	X
ARGON, ETC. AT CAVITY BOUNDARY		X		
NO SHOCK, OR WEAK LIMB SHOCK DETECTED				X

Table 2

II.6 SECONDARY OBJECTIVES

The Mercury interaction study will be strongly supported by measurements in interplanetary space and near Venus. As discussed above, proper interpretation of the Mercury encounter data requires detailed information about the interplanetary medium within 0.6 AU. The wind is highly variable, and we clearly cannot rely on the Helios measurements, made one or two years later, to clarify the state of the plasma at 0.4 AU in March of 1974. In fact, Helios will not have the real time telemetry capability of Mariner 1973, and the cruise waveform data potentially available from Mariner will provide unique and extremely valuable general information on the inner solar wind.

The Venus encounter analysis also strongly supports the Mercury study because the same wind-planet interaction may be found for both passes. The Venus interaction is generally understood, but several processes involving plasma waves remain to be explored directly. The Venus flyby speed is lower than that at Mercury and thus the Venus opportunity also provides a clear calibration for the payload with slower apparent changes in the various interaction features. In fact, if the payload can be operating during exit from the magnetosphere, the Mariner mission can use a single science payload to make comparative studies of the plasma environment surrounding Earth, Venus, and Mercury.

The plasma wave science requirements for the Mercury encounter lead to frequency ranges suitable for Venus, Earth, and the entire cruise portion of the mission, so that it is not necessary to include instrumentation uniquely designed for Venus or for the solar wind.

III. INSTRUMENT CONCEPT

III.1 INTRODUCTION

Instrumentation which is suitable for conducting a plasma wave experiment on the MVM'73 mission should consist of a boom-mounted sensor-preamplifier assembly and a body-mounted signal processing assembly. The sensor-preamplifier package would contain separate electric and magnetic field sensors along with associated preamplifiers. It should be boom-mounted so as to reduce the effect of spacecraft-generated interference. The preamplifiers serve to increase the signal amplitudes and transform the high sensor impedances to a level suitable for driving signals down the boom cable to the main electronics assembly. Signals from the boom package are then amplified and spectrum analyzed by the experiment's main electronics package, located in the science bay.

III.2 BOOM PACKAGE

The minimum VLF plasma wave experiment should consist of one E-field sensor and one B-field sensor oriented perpendicular to each other and mutually perpendicular to the spacecraft sun line. Three pairs of electric sensors, each representative of this concept, have thus far operated 20,000 hours as part of the OGO-5 payload. The E-field sensor consists of a 24-inch dipole antenna, with a preamplifier mounted at its geometric center. Threshold sensitivity for the E-field sensor of the type considered here is slightly frequency dependent, and it lies in the range 1 to 10 μV/m. The sensor, shown in Figure III.1, is a balanced capacitive dipole consisting of two spherical wire cages, each 12 cm in diameter, supported between the ends of a small fiberglass tube 0.5 meter in length. The spheres each have a capacity of 6.6 picofarads, and the cage form provides a low ratio of surface area to capacitance. A small surface area is desirable to minimize the unpredictable photo-electron coupling to the media. Each spherical cage is connected to one input of a differential preamplifier through an RFI filter which limits the effects of spacecraft radio frequency sources.

The B-field measurements are made using a search coil sensor consisting of several hundred thousand turns of fine wire centered on a 21-inch long, high permeability core which acts as a flux concentrator (see Figure III.2). The search coil sensor and preamplifier module are contained in a 1-1/2" x 1-1/2" x 24" electrostatic shield which can be used to house the E-field preamplifier. Threshold sensitivity for the B-field sensor is also frequency dependent and lies in the range 1 to 10 milligamma rms for a 2 kHz bandwidth, but levels down to 0.2 milligamma may be detectable. Triaxial coils of this type have accumulated more than 100,000 hours of successful operation on OGO's I-VI.

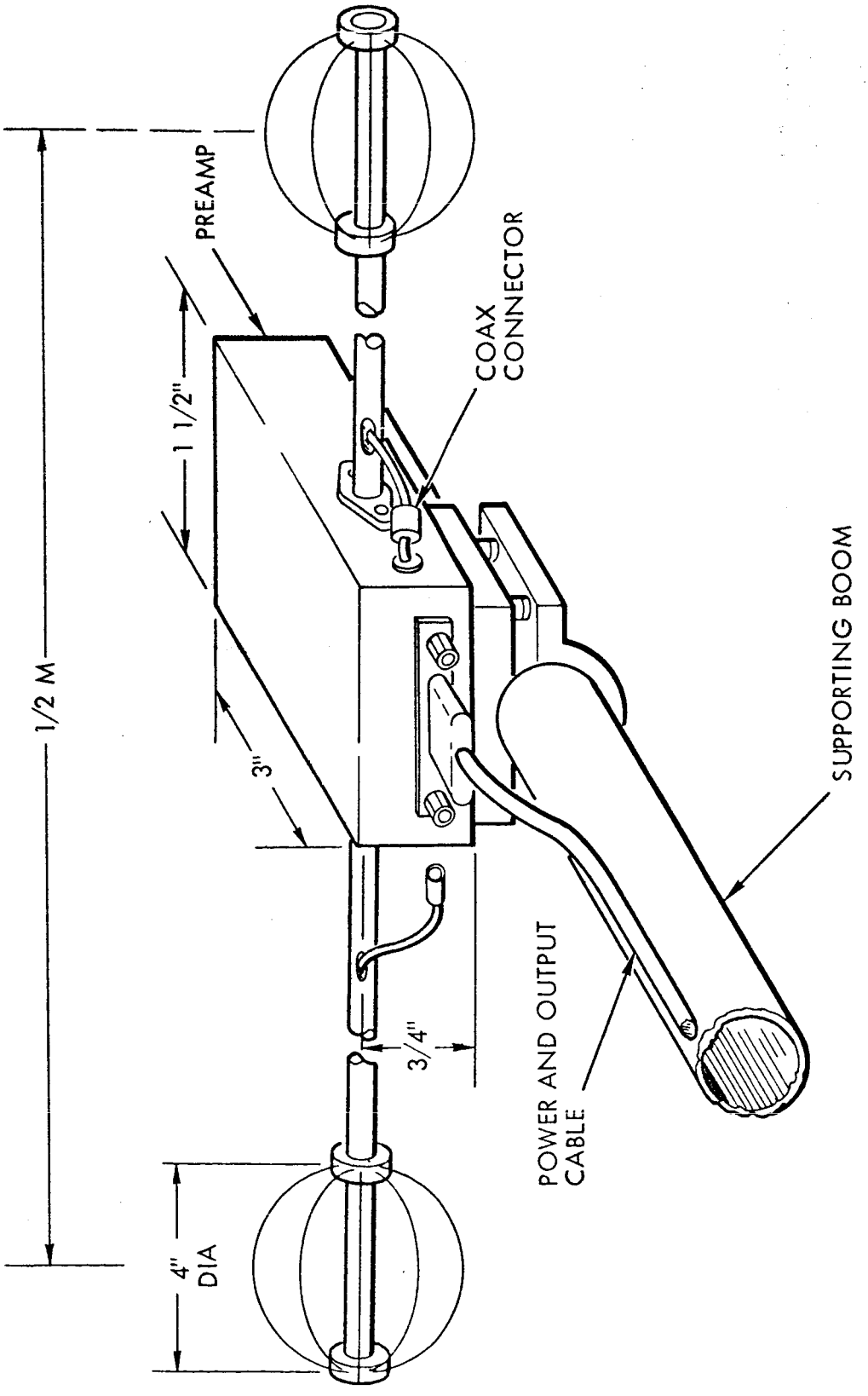
1/2 M
PREAMP
1 1/2"
COAX CONNECTOR
3"
SUPPORTING BOOM
3/4"
POWER AND OUTPUT CABLE
4" DIA

Figure III.1

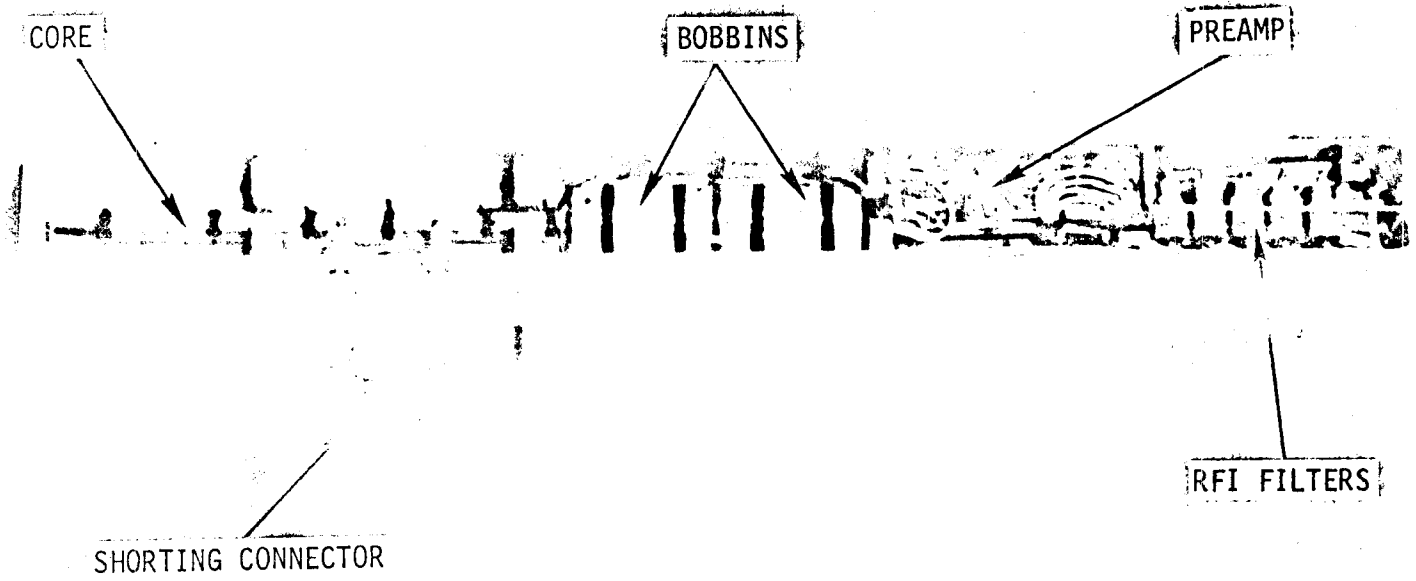

OGO-6 Sensor/Preamp Combination
(F-22 Search Coil Magnetometer Experiment)
OGO-6 Dimensions: 7/8" x 7/8" x 10-3/4"
MVM '73 search coil will be roughly in the same proprotions but about twice the size in all dimensions.

FIGURE III.2. OGO SEARCH COIL SENSOR

The preamplifiers have very high ($\approx 10^9\Omega$) input impedances and very low noise. They have differential inputs and outputs. The electric dipole common mode rejection is a function of input source impedance but is at least 40 db.

The coupling system connecting the preamplifiers and the main electronics is very critical if it is to be assured that no noise is introduced into the system on these conductors. In order to provide a dynamic range of 80 db or more, the minimum signal levels on these lines may be as small as tens of microvolts. Even using shielded twisted wire, noise signals can be introduced. However, if a differential amplifier is used at the input of the main electronics, the common mode rejection of this amplifier will reduce the susceptibility by as much as four orders of magnitude.

Figure III.3 shows a very desirable boom-mounting design developed by the MVM Project Team in response to the Plasma Wave Team requirements.

III.3 SIGNAL PROCESSING AND ELECTRONICS

A. General Description

The voltages induced in the electric and magnetic field sensors undergo amplification, filtering, and analysis in the experiment electronics package. The scientific desirability of obtaining simultaneous E and B measurements for all wave frequencies below the local electron cyclotron frequency implies that the assembly should contain two equivalent channels for $f \lesssim 2$ kHz. Ideally it would be desirable to simply digitize and transmit the broadband signal waveforms back to Earth. The signals could then be analyzed using sophisticated data processing equipment whose weight and power requirements exceed the spacecraft capability. The availability of waveform data would also keep all the various analysis options open to the experimenter, since the optimum method of analysis depends on the nature of the signal that is detected. The factor that restricts the bandwidth of the signals that are transmitted is simply the available telemetry bit rate. Under circumstances where it is not practical to exploit extreme broadband capability of the E-field and search coil sensors, a compromise involving on-board analysis is necessary. Of the various alternatives the one which appears to have the most universal appeal is frequency analysis using a multichannel spectrum analyzer. Thus the basic instrument was considered to provide two types of output, broadband waveforms where highest frequencies would be compatible with the telemetry rate, and the outputs of two spectrum analyzers that would cover the remaining high end of the frequency range. The basic block diagram is shown in Figure III.4.

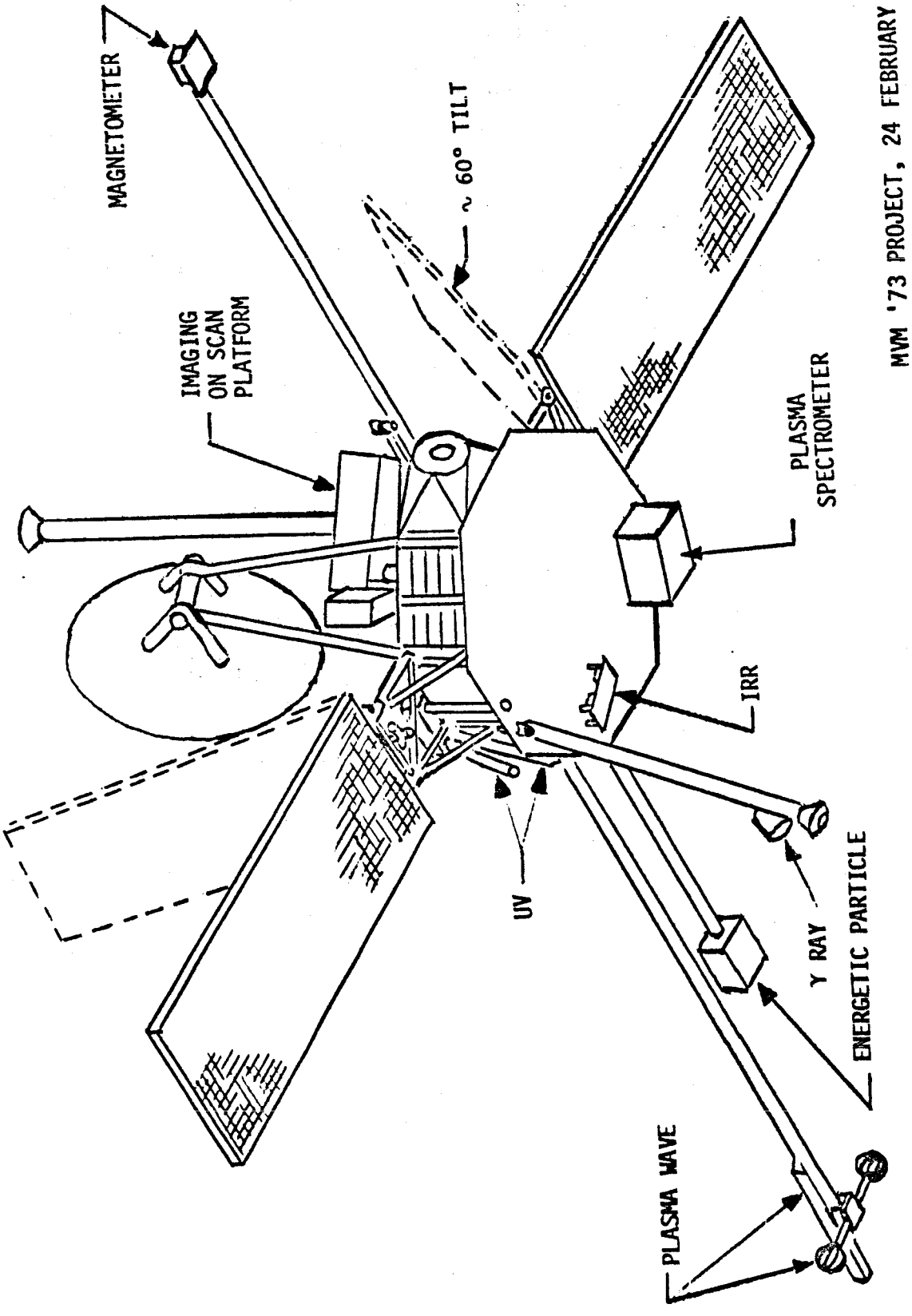

MVM '73 PROJECT, 24 FEBRUARY 1970

Figure III.3a

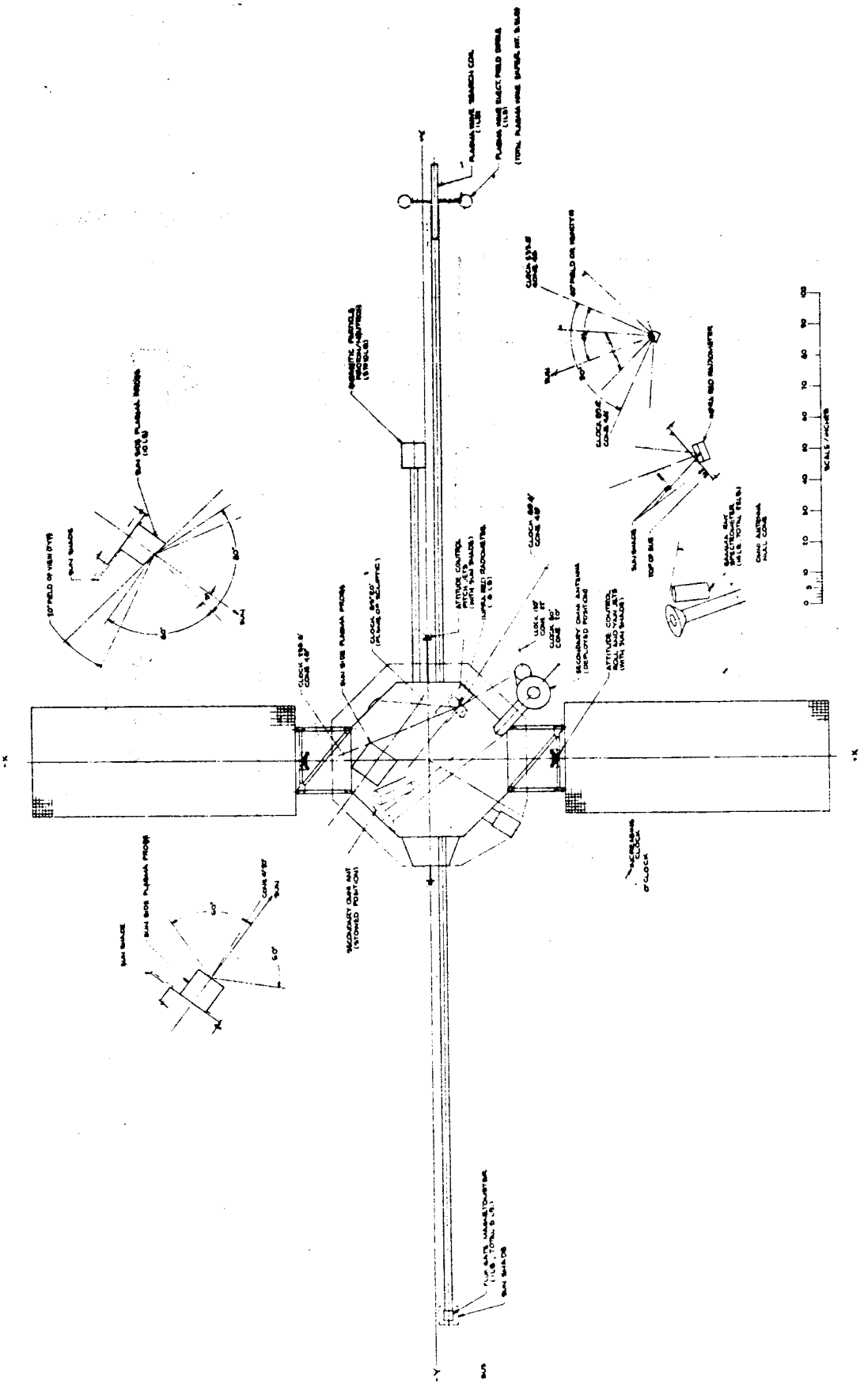

Figure III.3b

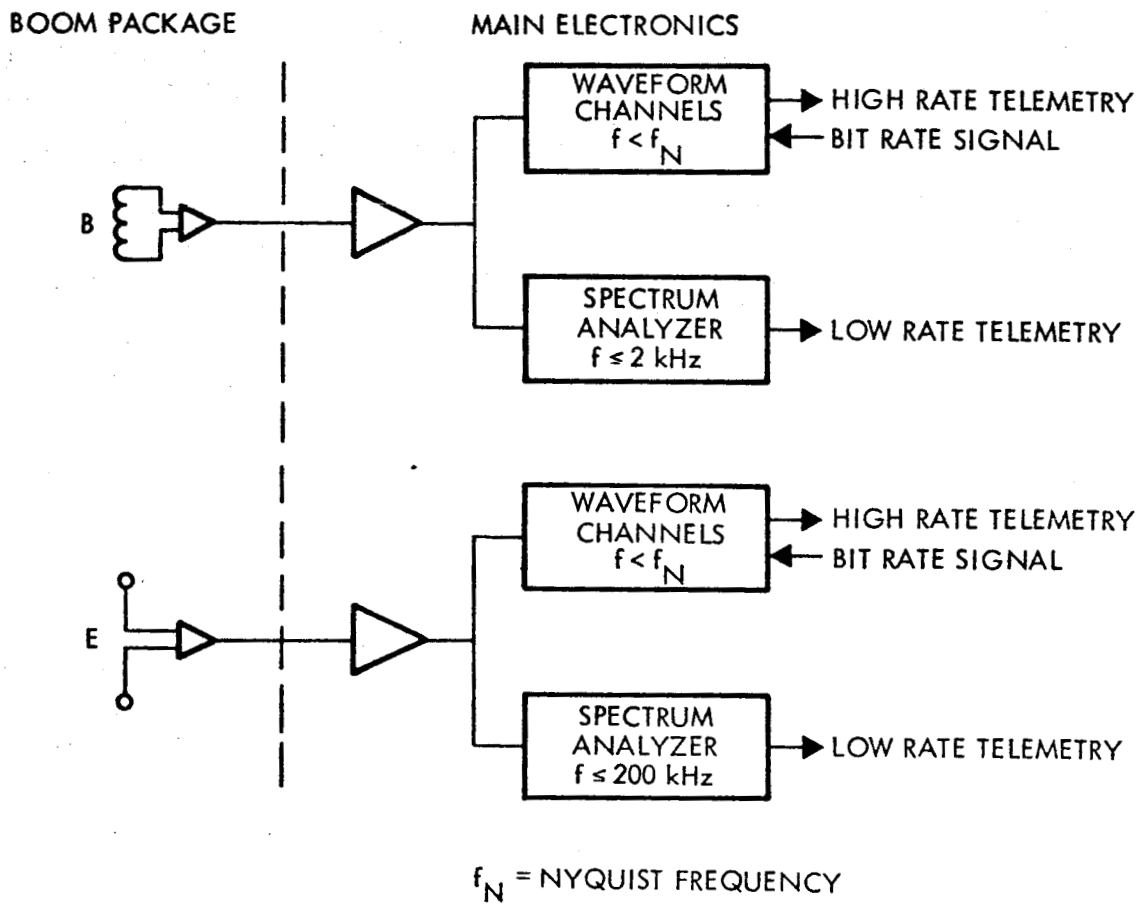

f_N = NYQUIST FREQUENCY

Figure III.4

Figure III.5 contains an OGO-5 example of the different output forms. Here the lowest panel gives the variation in the level of a single channel from a multi-channel spectrum analyzer. The bow shock is easily detected, but details are clearly lacking, and it is not possible to ascertain whether the minimum level is produced by a physical ambient signal or a local limitation. The top panels illustrate the great increase in resolution available when broadband waveform data are transmitted. The spacecraft interference line at 2.461 kHz is clearly evident in the central frequency-time diagram; the multiple shock structure is also well defined, and upstream noise bursts are clearly present.

The outputs from the spectrum channels can merely be processed using standard statistical techniques, but waveform data can be analyzed in many ways. The top panel in Figure III.5 shows an expanded version of the spectral analysis in which each sweep is 50 milliseconds apart. This kind of high time resolution capability will be especially vital for the Mercury encounter where the shock crossing time can be much less than 100 milliseconds. Moreover, the plasma probe may take about 30 seconds to do one angular scan, and the upper panels show that much E and B information can be accumulated during this time if waveform transmissions are available.

If high rate waveform data are available, then other ground-based processing schemes can be used. For instance, E and B correlation studies can be performed in the laboratory. Moreover, since the waveform data represent measurements of audio-frequency oscillations, analog tapes can be written and audio analysis techniques can be employed. In fact, many orderly patterns are recognizable when tapes of shocks, chorus, hiss, magnetosheath emissions, etc. are simply transmitted through audio frequency systems.

B. Broadband Receiver

The purpose of the broadband receiver shown in Figure III.4 is to condition electric and magnetic field signals for very high rate sampling by the spacecraft telemetry system. With the use of the 210 ft DSN receiving antenna bit rates as high as 16 to 48 Kbits/sec are possible during the direct transmission portions of the Venus and Mercury encounters. Since many of the other experiments require much lower bit rates during encounter it is believed that the majority of this telemetry rate can be made available to the plasma wave experiment. With this high bit rate it will be possible to transmit broadband (up to 1 kHz) electric and magnetic field waveforms to the Earth for very high time resolution frequency spectral analysis. This technique of direct transmission of broadband waveforms has proven to be of great value on previous plasma wave experiments such as on the Alouette, Injun and OGO satellites. As noted above, by transmitting the waveforms directly to the ground, much more sophisticated data processing

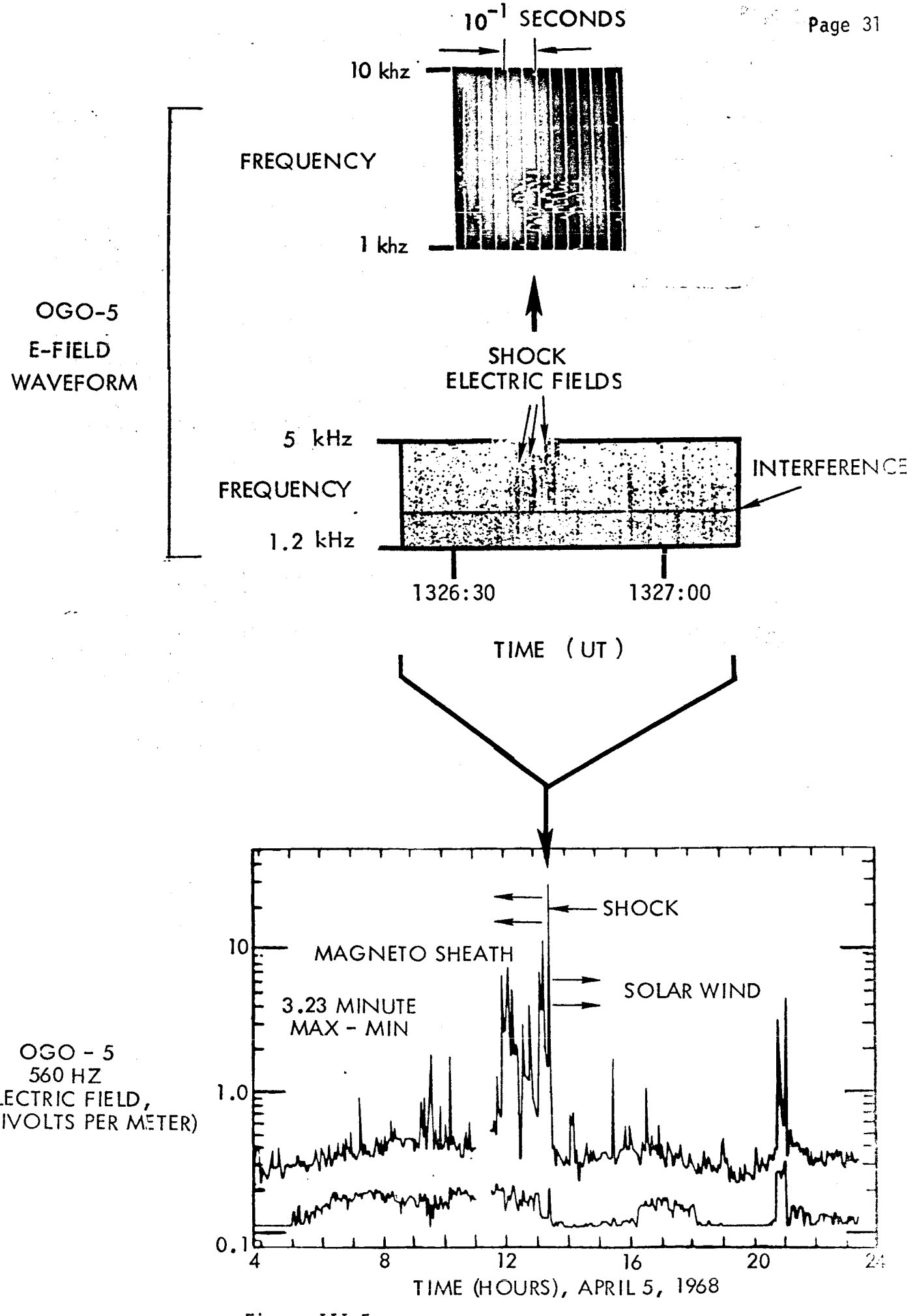
10^{-1} SECONDS
10 khz
FREQUENCY
1 khz
OGO-5
E-FIELD
WAVEFORM
SHOCK
ELECTRIC FIELDS
5 kHz
FREQUENCY
1.2 kHz
INTERFERENCE
1326:30
1327:00
TIME (UT)
SHOCK
MAGNETO SHEATH
SOLAR WIND
3.23 MINUTE
MAX - MIN
10
1.0
0.1
4
8
12
16
20
TIME (HOURS), APRIL 5, 1968
OGO - 5
560 HZ
ELECTRIC FIELD,
(MILLIVOLTS PER METER)

Figure III.5

techniques can be used than are possible with satellite-borne instrumentation. In fact, the broadband receiver instrumentation is considerably simpler than a high resolution multichannel spectrum analyzer covering the same frequency range, which would be desirable if high rate waveform sampling is not employed. It is therefore recommended that the frequency coverage of the broadband receiver be extended to as high a frequency permitted by the telemetry and that narrowband spectrum analyzer measurements be made only above the highest frequency covered by the broadband receiver.

Because of the extremely large dynamic range of the field amplitudes the broadband receiver must amplitude compress the received signals to a dynamic range suitable for high data rate waveform transmission. This amplitude compression could be accomplished by either a nonlinear logarithmic ac amplifier or an automatic gain control (AGC) circuit. It may also be desirable to divide the frequency range into two or more adjacent broadband channels to reduce the susceptibility of the broadband receiver system to strong interference in a limited frequency range. Low rate amplitude measurements in these broadband channels could provide crude spectrum measurements during earth occultation and other periods when high data rate telemetry is not available.

C. Spectrum Analyzer

The spectrum analyzers are to provide a continuous survey of the electric and magnetic field amplitudes over a large frequency range with a low bit rate. A frequency resolution of 100 percent ($\Delta f/f_o$), a time resolution of 1 second, and a six bit amplitude word should be adequate. During Earth occultation only the spectrum analyzer data need be stored for later transmission.

An appropriate frequency range for the magnetic field measurement is 10 Hz to 2 kHz. The lower limit is determined by the proposed upper limit of the fluxgate magnetometer and the upper limit is set by the maximum expected electron gyrofrequency (see Figure II.2, which shows the gyrofrequency vs distance from the Sun). A lower limit of 0.01 Hz is chosen for the electric field to cover long period changes in the electric field and the upper limit of 200 kHz is chosen to be above the maximum expected plasma frequency (see Figure II.2).

Amplifiers which give both the average and the peak field strengths during the sampling period are suggested. Compressor amplifiers can have a 100 db dynamic range and a time constant of one wave period.

It is recommended that the frequency range be segmented by filters spaced approximately every half decade. Each one of the filters is followed by a compressor amplifier. Therefore, every sample period the

rms and peak amplitudes for that sample period over the frequency range are obtained. The peak detectors are particularly important for capturing the planetary shock frequency spectra and other transient phenomena even though they may occur in a time less than a sample period.

At the lowest frequencies the integrated amplitude from the active filter channels used in the broadband receiver can be read out. At the higher frequencies passive LCR filters can be easily utilized.

The resulting data from the spectrum analyzers can be processed to produce peak amplitude and rms amplitude frequency-time diagrams for the electric and magnetic fields.

III.4 INTERFACE REQUIREMENTS

Based on our OGO experience, we feel that the experiment electronics could probably be fitted into a housing with typical maximum dimensions of 6" by 7" by 4". A weight of 3.5 pounds appears practical for the amount of data processing contemplated above. The boom-mounted sensors and preamplifiers should have a total weight less than two pounds. Some care should be exercised in mounting the sensors and the main assembly; it would be very desirable to electrically isolate both the boom package and the electronics from the spacecraft structure in order to ensure the integrity of the instrument grounding and shielding. This has important implications for electromagnetic compatibility between the experiment and the spacecraft. Power to operate the experiment could be derived from either ac or dc spacecraft power. In either case, 3.5 watts appear to be adequate for the system described above. Several commands might be needed to turn the ON and OFF and to activate an in-flight calibration sequence. Since the frequency response of the waveform channels would be determined by the prevailing telemetry rate, some form of bit rate signal would be needed to control the upper cutoff frequency of the variable bandwidth amplifiers. The scientific data could be in the form of binary numbers from a shift register, analog voltages, or an intermediate such as modulated-width pulses. If the outputs from the spectrum analyzer filters were commutated, the output data would require only four lines in order to be routed to the spacecraft data system (as shown in the block diagram (Figure III.4).

The real time and stored wideband telemetry requirements are flexible. The plasma wave detector is basically a processor of analog signals, and it would even be useful to examine frequencies as high as 100-200 kHz directly. Using 4 to 6 bit words, it is clear that the experiment could

thus benefit from the 650 kb/sec real time capability, and bursts of high rate stored data would also be valuable. This type of experiment might be regarded as a sink for telemetry, in a very real sense.

The data processing costs will, of course, go up with the total number of bits analyzed. However, the proposed low rate spectrum analyzer mode will lead to rapid identification of those time periods of greatest interest, and the detailed processing of high rate data can be confined to these times.

The dual occultation trajectory shown in Figure II.6 illustrates that many of the important Mercury interaction features (shock, cavity boundary, cavity, second boundary crossing) will be encountered before Earth occultation. The data from the plasma wave detector should be most important for this early period with real time high rate telemetry. Therefore, we feel that this experiment does not have an unusual storage requirement for the earth occultation portion. If only the spectrum analyzer output is stored at the nominal cruise rate ($\sim$ 230 bits/sec) for fifteen minutes, then the total storage of 2×10^5 bits gives very detailed spectral information. More would be desirable, but even a smaller occultation storage is tolerable and useful.

The instrument concept described here assumes that the sensors will be boom-mounted. During the SSG deliberations we first considered other mounting schemes, and the booms shown in Figures III.3a, III.3b are the final outgrowth of an interim dummy solar panel configuration. These booms should accordingly be considered part of the spacecraft, and their costs should not be charged to the experiments mounted on them.

III.5 QUALITY ASSURANCE

The members of the Plasma Wave Experiment Team recognize the great importance of an adequate Quality Assurance and Reliability Assurance Plan to the success of any flight program. They also recognize that it is cost-ineffective to impose greater QA and RA documentation requirements than those necessary to assure QC and reliability, since these costs reduce the design and fabrication budget without adding to the final reliability figure of the flight experiment. Thus, we suggest that the investigator choose a QA and RA plan which has been found to be successful, but would be significantly less costly than the full Mariner-type QA and RA documentation requirements. We believe justification for such a modified plan can be based on the flight record of the scientific experiments. We describe below some such examples from the experience of the study team members.

The plasma wave experiment recommended combines a search coil magnetometer and a short electric dipole sensor. These two sensors and their associated electronics have remarkable flight records on several spacecraft. The JPL/UCLA search coils on OGO's I through VI have operated either for the entire life of the mission or are still operating without any type of failure for more than 100,000 hours (11.3 spacecraft years), while the TRW plasma wave detector experiment (tri-axial electric dipoles and tri-axial air-core loops) on OGO-V is still operating after more than 18,000 hours in orbit without a malfunction. In addition, the University of Iowa magnetic loop (Injuns 3,5) and electric dipole (Injun 5) plasma wave experiments have operated for more than 4,000 hours with no failures even though these experiments have been turned on and off by ground commands a great many times.

These very successful flight records for the plasma wave experiments are due to the experimenters' appreciation for an adequate Quality Assurance, Reliability Assurance, and Inspection Procedure which is consistent with the cost limitations of the flight program. In the case of the Mariner-Venus-Mercury 1973 program where costs are a primary consideration, we recommend a QA, RA and Inspection Procedure similar to that used by the plasma wave experimenters involved in the OGO-I through VI programs, since it would be far less costly than the full Mariner QA, RA and Inspection requirements, while on the basis of the flight records cited above, it is clearly sufficient to produce reliable flight hardware.

The recommended QA Plan thus would be based upon following the appropriate sections of NASA NPC 200-2, and NPC 200-3 for QA and Parts Inspections, and NPC 250-1 for RA Provisions. This Plan should be generated by the experimenters, invoking those provisions of the cited documents which they have found by experience provide adequate assurance; this Plan should then be approved by the MVM'73 Project after suitable negotiations.

IV. EMC CONSIDERATIONS

IV.1 GENERAL SPECIFICATIONS

The E and B sensors described in Section III are capable of detecting VLF signals as small as about one microvolt/meter and 0.2 milligamma, respectively, in narrow bandpass channels. However, plasma wave measurements made near the Earth's bow shock, and magnetosheath (ion acoustic waves and whistler emissions), and in the magnetosphere (chorus and electrostatic noise bursts) typically involve much stronger signals with $\Delta E \simeq 500$ μV/meter to 50 millivolts/meter and $\Delta B \sim$ 2-20 milligamma. If strong Earth-like bow shock crossings, or similar chorus-like emissions are detected during the Mercury and Venus encounters, then the ambient plasma wave amplitudes should be readily detectable over any moderate spacecraft noise signals. This is especially likely to be true for the Mercury encounter because the ambient wave amplitudes increase with increasing plasma temperature and imbedded field strength (i.e., with decreasing distance to the Sun).

However, near Mercury (and Venus) the wave experimenters may be examining weak limb shocks, novel wave excitation patterns, and signals propagating from non-local sources. During this study, we therefore considered a modest but effective EMC program aimed at keeping the VLF noise levels at the sensors down to about 2 milligamma (rms) broadband for B, and 10-100 μV/meter (rms) narrowband for E. We recognize that Mariner '73 is a fund-limited program largely based on existing spacecraft and subsystem designs, and that no extensive new EMC program can now be contemplated. Nevertheless, the ultimate sensor threshold levels mentioned initially should be regarded as desirable goals that are particularly significant for the cruise portion of the mission.

During the SSG planning phase we proposed a number of specific spacecraft design changes that would naturally enhance the compatibility of a VLF wave experiment with Mariner '73, and many of these plans are now in the baseline mission design, or can be incorporated with relative ease.

a. The most important defense against interference is the use of a boom. The sensor mounting shown in Figure III.3 will greatly reduce any effects of spacecraft noise signals on the sensors.

b. Interference coupled through the plasma is primarily due to ac fluctuations on the solar panels and on exposed experiment grids and collectors. We have recommended filtering of the solar panels (see Section IV.2). We also recommend insulating all current-carrying wires external to the spacecraft, and addition of grounded outer grids to experiments producing ac noise.

c. We recommend that plasma wave experimenters minimize conducted interference by filtering all lines coming in to their experiment box. Wherever possible, all spacecraft power supply and modulation frequencies should exceed 2 kHz, and should preferably be synchronized.

d. The plasma wave electric field sensor should be a balanced dipole, mounted symmetrically (see Figures III.1, III.2). The spacecraft shell should also be a continuous electrostatic shield.

e. The use of magnetic and electric shields on electrically-driven motors and solenoid valves is recommended.

f. We recommend the use of twisted, shielded pairs for leads to experiments and subsystems and the development of a single-point spacecraft ground system that eliminates ground loops.

g. Grounding procedures for the experiment booms and other appendages (e.g., solar panel frames) should be set up in accordance with the desires of the plasma wave experimenters.

We also feel that the use of a high data rate, leading to acquisition of waveform data, will allow the wave experimenter to tolerate some moderate interference signals. These can readily be recognized and removed during the data processing phase. Certain EMC tests should also be performed during the integration activities, and recommended procedures are discussed in Section V.

IV.2 SOLAR PANEL FILTERING

Experience with numerous satellite ac electric field experiments has shown that one of the primary sources of interference is from ac noise voltages on the spacecraft solar array. These noise voltages are generated by power supply switching transients, motors, and other miscellaneous sources within the spacecraft, and conducted out to the solar array via the power system. Since these noise voltages may easily have amplitudes as large as 1 volt rms in the frequency range of interest (1 Hz - 100 kHz), and the electric field experiment can detect antenna voltages on the order of 1 μV, it is evident that serious interference can be expected if no special precautions are taken.

Two types of coupling from the solar array to the electric field sensors can be distinguished.

a. Direct Coupling. Direct coupling is due to the near field (primarily electrostatic) generated by the ac voltages on the solar array. Since the near field intensity decreases rapidly with increasing distance from the source, it is desirable to locate the electric field sensor as far as possible from the solar array to minimize the direct coupled interference from the solar array, and this is one justification for the boom of Figure III.3.

b. Common Mode. Since the solar array cells are capacitively coupled to the plasma surrounding the spacecraft, any noise voltages on the solar array will cause comparable variations of the spacecraft potential relative to the plasma potential. These variations in the spacecraft potential produce common mode interference signals into the electric field sensor. Since the electric field is proportional to the potential difference between the electric field antenna elements, these common mode interference signals must be suppressed. Because of unknown and variable differences in the sheath characteristics of the two antenna elements, the common mode suppression which can be achieved is probably limited to about 40 db or less. Since this common mode coupling arises because of variations in the spacecraft potential, this type of interference is not greatly reduced by increasing the length of the boom on which the electric field sensor is mounted. This type of interference can primarily be reduced by decreasing the noise voltages on the solar array. Since a voltage sensitivity of about 1 μV can be achieved for the electric field preamplifiers, and only about 40-60 db of common mode attenuation is possible, it is necessary to maintain the noise voltages on the solar array below about 1 mV to 100 μV over the frequency range of interest to completely eliminate common mode interference. However, as noted in Section V.1, somewhat larger interference levels than this are tolerable.

A design goal solar array noise level of 1 millivolt rms from 10-300 Hz, and 0.1 millivolt rms from 300 Hz to 200 kHz is recommended on the MVM'73 mission. This noise level, although small, is achievable with

realistic filtering between the power system and the solar array. These levels were achieved on the NASA/University of Iowa Injun 5 satellite using the pi-section filter shown below:

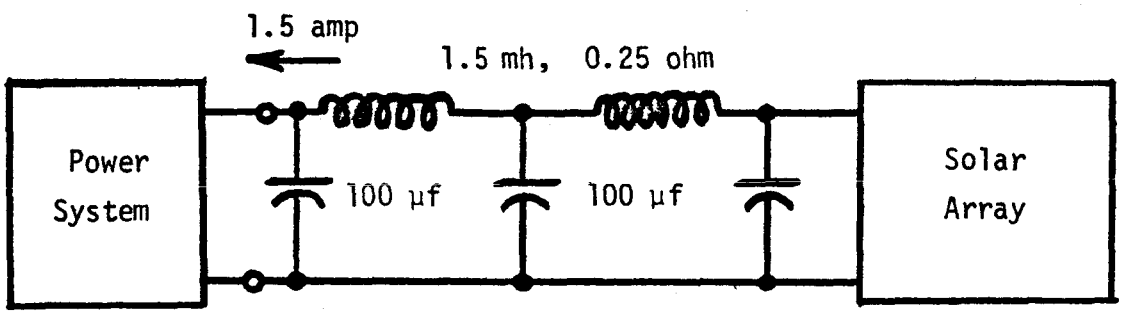

These specifications have also been used for the design of the IMP-I, H, and J power system. On these spacecrafts the current from the solar array is approximately 5 amp, which is considerably more than for the Injun 5 system and more comparable to the Mariner power system requirements. For these larger currents, it is difficult to avoid saturating the inductor core with an associated reduction in the differential inductance. This difficulty was partially solved on IMP-I by using two windings on the same core with the direction of the winding such that the dc magnetic bias field in the core is zero, as shown below.

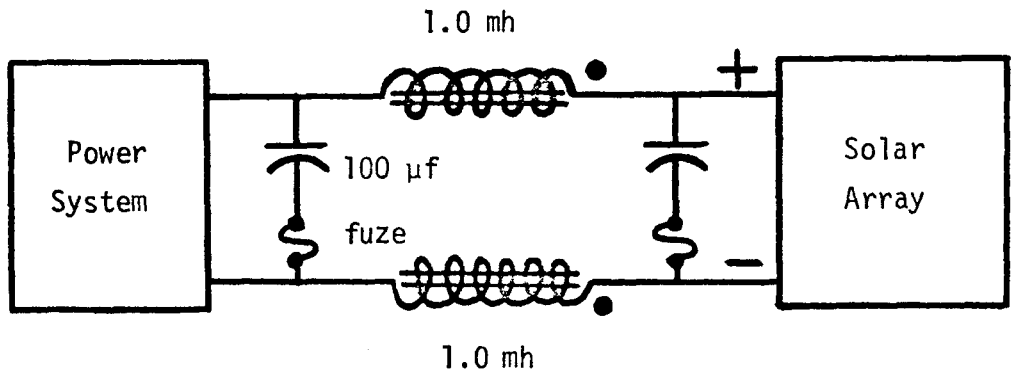

This system provides excellent attentuation for common mode voltage coupling from the power system to the solar array, and somewhat reduced attentuation for differential voltages on the (+) and (-) power buses (because of the

mutual coupling between the winding). Actual performance information is not yet available for the IMP-I solar array filter. It is expected that the IMP-I solar array filter will come close to meeting the noise specification given above.

V. TEST PLAN

V.1. SUBSYSTEM AND SYSTEM LEVEL TESTS

INTRODUCTION

One aspect of prelaunch testing is common to all spacecraft carrying sensitive wave experiments. That is the need to ensure that electromagnetic fields of spacecraft origin do not exceed levels which would jeopardize the principle science objectives of the experiments. However, the kind of testing appropriate to the MVM '73 mission must reflect the following facts.

a. Spacecraft subsystem functional designs will be very nearly the same as Mariners '71 and/or '69. These designs in turn represent evolutionary changes from earlier Mariner missions. Interference problems uncovered during EMI testing must be resolved by simple means, perhaps not ideal, in order to avoid the cost increases associated with major redesign of subsystems.

b. The principle science objectives for the MVM '73 mission entail making measurements in the vicinity of Mercury where the naturally occurring plasma waves are expected to be comparatively large in amplitude. A level of spacecraft interference which is acceptable for Mercury measurements may still be so large that it becomes difficult to obtain good quality, low level interplanetary data for all but a small fraction of the time. However, this should still be considered an acceptable situation because the interplanetary measurements have been designated as secondary objectives; moreover, the high cruise telemetry rate capability of MVM '73 will enable the plasma wave experiment to accumulate many examples of the large amplitude waves and shocks that regularly occur in the interplanetary medium. (Note the levels of the intense solar wind noise bursts at 2045-2100 UT in Figure III.5.)

c. The plasma wave sensors on the MVM '73 baseline spacecraft are to be sufficiently far removed from the main spacecraft so that only sources of high levels of electromagnetic interference should be sought out by the EMC test program. This will hold down the costs of the test program. Such an approach is a consequence of the fact that the boom length itself is the first line of defense in avoiding EMI problems.

SYSTEM EMC TESTING

The standard EMC program, which has been a part of previous Mariner projects, will partially satisfy the needs of a plasma wave experiment. For the TRW electric field detector on Pioneer 8, 9, E no additional tests were instituted, and in-flight interference proved to be no problem. However, it is desirable to consider augmenting the program by including two additional systems tests and by extending the range of field measurements down to very low frequencies. One of the systems tests would be designed to uncover conducted interference; the other, to test for radiated interference.

a. Conducted Interference

The conducted interference test will involve observing the plasma wave experiment outputs as the spacecraft is exercised through its various operating modes in the systems test building. Here the experiment sensors would be desensitized and shielded, or completely shorted out so as to be immune to radiated interference. This amounts to defining conducted interference as encompassing all unwanted voltages (exclusive of instrument noise) which enter the experiment's data channels by any means other than radiative fields acting upon the sensors. Included in this definition are:

1) Broadband noise and voltage spikes fed to the experiment on spacecraft interface lines.

2) Crosstalk in the experiment data channels from adjacent conductors in spacecraft harnesses.

3) Spurious demodulation of out-of-band RF signals that are coupled into the experiment by means other than through the sensors.

This definition of conducted interference many not coincide with the customary interpretation by EMC groups, but the reason it is used here is that the same systems test can be used to uncover problems in all three areas listed above.

b. Radiated Interference

The systems test designed to uncover radiated interference will require a well controlled electromagnetic environment in the test area, as opposed to the conducted interference test which may be performed in the normal operating

environment of the Spacecraft Assembly Facility. Even when elaborate precautions are taken, systems level measurements of low frequency electric and magnetic fields will be difficult to perform in an assembly building. On other projects spacecraft have been transported to remote facilities. The spacecraft have then been battery-operated in a mode free of hardline connections and RF linked to a systems test complex, some distance away. In the case of MVM '73 this should not be necessary because:

1) Some of the short duration signals in space are expected to have sufficient amplitude and to occur often enough that, given the high Mariner data rates, a plasma wave experiment will accumulate an adequate statistical sample of these, even if smaller waves are frequently masked by spacecraft EMI.

2) The long experiment boom makes it possible to conduct a radiated interference test using multiple sensors located along the boom and near the spacecraft. By employing additional sensors, closer to the sources of EMI, a higher level of background noise can be tolerated since the radial dependence of the interference can be inferred from the measurements and the resulting field strengths at the plasma wave sensor location computed.

However, the higher level of tolerable background radiation is by no means as large as that typical of most test complexes. In order to perform a system level radiative interference test in a spacecraft assembly building, it will be necessary to satisfy the following conditions:

1) Conduct the tests late at night with all commercial power to the building turned off, using only battery-operated lanterns for illumination of the test area.

2) Battery-operate the spacecraft in essentially a free mode configuration using only a minimum number of hard line connections to monitor the condition of the spacecraft with battery-operated, inverter-free, monitoring equipment

3) RF link the spacecraft telemetry outputs to the systems test complex, located in another building.

4) Provide command capability using an RF link from the test complex to the spacecraft command receiver.

SUBSYSTEM EMC TESTING

Introduction. The testing of subsystems for electromagnetic compatibility with a plasma wave experiment will principally involve making ac magnetic field measurements. A few ac electric field measurements may also be useful, but these will be exceptional cases, since most subsystems are contained within the conducting skin of the spacecraft, and most experiments are contained within a conducting chassis connected to spacecraft ground potential. One obvious exception to this philosophy is the solar array subsystem which is not completely enclosed by a conducting layer. This is why adequate solar panel filtering (10 Hz $\leq$ f $\leq$ 100 kHz) is an important design consideration.

AC Magnetic Field Tests. The extent to which subsystems are mapped for ac magnetic fields will depend upon the adequacy of the systems level EMC tests adopted by the project. If the radiated EMI systems test, outlined in the previous section, is adopted, then only those subsystems which are found to be a problem will need to be tested further at a controlled environment facility where the radiative EMI problems can be resolved.

For new experiment packages or subsystems that are being redesigned it might be useful to consider imposition of a moderate design constraint. The constraint should state the maximum allowable ac magnetic field at a specified distance and be backed up by measurements that are included in the acceptance test procedure. Since the scientific objectives of the plasma wave experiment require a B-field noise threshold in the 1 to 2 milligamma range, it is reasonable to hope that spacecraft-caused interference will not exceed this amount in the frequency band 10 Hz to 2 kHz. In order to achieve 2 mγ rms at the search coil sensor, a representative subsystem specification might require that a package generate no more than 0.1γ rms at 3 feet. As an example of what this means in terms of currents flowing in a single turn loop, 0.1γ rms would be measured from a square loop of wire, 1 foot on a side, carrying 4 milliamperes rms of noise on a 2 kHz band. For discrete frequency interference the 0.1γ rms subsystem specification would convert to a number like 2 milligamma rms at 3 feet, 10 Hz $\leq$ f $\leq$ 2 kHz.

The measurements required to verify compliance with such ac magnetic specifications would probably require two levels of testing. The first (and perhaps only) test would be included in the routine acceptance test procedure. It would involve making ac field measurements in a rather unfavorable environment (and maybe late at night) using a differential sensor arrangement to minimize the effect of uniform ac fields in the test area.

This test would amount to "sniffing" an operating subsystem with an ac gradient probe, paying due attention to the proximity of the subassembly's bench test equipment and associated cables. If the tests show that the package may be a source of interference to the search coil, then a second test would be scheduled in a more favorable environment, say within a magnetically shielded room. Here, with the cooperation of subsystem designers, the problem could hopefully be resolved.

V.2. IN-FLIGHT TESTS

Testing in flight provides a final and valuable search for interference with the field-measuring equipment. Each field-measuring experiment should be turned on first with all other experiments inoperative and with the minimum number of essential spacecraft systems activated. At this point the other experiments and spacecraft functions should be turned on in sequence, allowing sufficient time to obtain a complete record of the signal change associated with each operation.

This test is important because it allows the experimenter to identify the measured wave levels that represent detection of ambient signals. If one or more channels are found to have enhanced background levels due to interference, then only signals above these levels will be interpreted as ambient. In many cases, it can be established that the interference is greatly reduced when the spacecraft or experiments are in some particular command state; occasionally it is then possible to adjust the mission profile (with time sharing, for instance) to provide more interference-free data.

The in-flight interference test is particularly important when waveform data are to be processed. The conventional spectral display is a frequency-time diagram, and since the interference tones are generally narrowbanded and constant in frequency, they appear as narrow horizontal lines (see central panel in Figure III.5). If these spurious lines can be identified early in the flight, then digital filters can be inserted in the data reduction process to eliminate the lines. This is particularly important if quick-look spectral processing (f-t diagrams or audio analysis) is planned for the planetary encounter. In this case, a full-scale in-flight "dress rehearsal" of the encounter is recommended.

VI. REFERENCES

Bratenahl, A., and C. M. Yeates, Experimental study of magnetic flux transfer at the hyperbolic neutral point, Phys. Fluids, in press, 1970.

Cloatier, P. A., M. B. McElroy and F. C. Michel, Modification of the Martian ionosphere by the solar wind, J. Geophys. Res., 74, 6215, 1969.

Colburn, D. S., R. G. Currie, J. D. Mihalov, and C. P. Sonett, Diamagnetic solar wind cavity discovered behind moon, Science, 158, 1040, 1967.

Fredricks, R. W., G. M. Crook, C. F. Kennel, I. M. Green, F. L. Scarf, P. J. Coleman, Jr., and C. T. Russell, Electrostatic turbulence in bow shock structures: OGO-5 observations, J. Geophys. Res., in press, 1970.

Paul, J. W. M., C. C. Daughney, and L. S. Holmes, Study of turbulence within a collisionless shock using collective scattering of light, Culham Laboratory Report CLM-P222, 1969.

Sonett, C. P., and D. S. Colburn, The principle of solar wind induced planetary dynamos, Phys. Earth Planet. Interiors, 1, 326, 1968.

Scarf, F. L., Plasma instability and the microwave radiation from Venus. J. Geophys. Res., 68, 141, 1963.

APPENDIX 1

MERCURY SURFACE ELECTRICAL PROPERTIES

1. Measurements Which Can Give the Surface Electrical Properties

Four types of measurements have been used to obtain estimates of the lunar surface electrical properties -- the dielectric constant and the electrical conductivity [England et al., 1968]. These measurements are:

a) Laboratory studies on electric properties of lunar type rocks;

b) Thermal inertia determined during lunation and at eclipses;

c) A comparison between infrared and microwave temperature fluctuations;

d) Radar reflection.

Measurement a) yields a best estimate of the electrical conductivity at 10^{-6} (ohm meter)$^{-1}$, which is appropriate for the near surface and similar to that of rock in which ice fills the pores. Measurements b), c), and d) have been combined to give an electrical conductivity of 6.5×10^{-2} (ohm meter)$^{-1}$, and measurement d) gives a relative dielectric constant of 2.8. England et al. [1968] conclude that this value of conductivity (comparable to highly conducting moist soil) is an overestimate probably due to the failure to account for all the loss mechanisms of electromagnetic energy (radar reflection). Such loss mechanisms include resonance absorption and scattering.

Of these four types of measurements apparently only the radar reflection can be used at present to deduce the electrical properties of Mercury. The type of surface rock is relatively unknown, and Mercury is too close to the sun and too far from the earth to make reliable measurements of the thermal inertia and of the microwave and infrared temperature fluctuations. Taking the Moon as an example, the radar reflection data should give an overestimate of the electrical conductivity.

2. Radar Reflection Data on Mercury

Radar data on Mercury are summarized by Evans and Hagfors [1968]. These data are of two types: 1) the reflected power which gives the radar cross section compared to the geometric cross sections as a function of wavelength, and 2) the time delay of short pulses which gives the angular scattering distribution. Measurements of the radar cross section are plotted in Figure 1.1 for wavelengths of 3.8 cm to 70 cm. The average value of the cross section is about 6 percent, with only a slight wavelength dependence indicating an increased cross section at longer wavelengths. Variations of the cross section with time have not been reported (all data were taken near inferior conjunction, however). The cross section of Mercury is slightly lower than that of the Moon, which suggests that the surface is also porous, or unconsolidated. Short pulse studies of Mercury indicate qualitatively that Mercury is somewhat rougher than the Moon (which is rougher than Venus).

3. Upper Limit to Value of Surface Dielectric Constant and Electrical Conductivity

The radar cross section as a function of wavelength depends on the surface electric properties and on the scattering distribution. From the short pulse data some knowledge of the scattering distribution can be obtained so that an estimate of the electrical properties can be made.

Specifically, the radar cross section can be written [Evans and Hagfors, 1968]

$$\frac{\sigma}{\pi a^2} = g\,\rho_o \tag{1}$$

where g is the directivity factor which expresses the gain due to scattering, ρ_o is the power reflection coefficient at normal incidence, and a is the radius of Mercury. The power reflection coefficient can be given explicitly in terms of the electric and magnetic properties

$$\rho_o = |Q|^2 \tag{2}$$

$$\text{where } Q = \frac{1 - \frac{1}{\mu_r}\left(\varepsilon_r + i\frac{s}{\omega\varepsilon_0}\right)^{1/2}}{1 + \frac{1}{\mu_r}\left(\varepsilon_r + i\frac{s}{\omega\varepsilon_0}\right)^{1/2}} \tag{3}$$

and μ_r is the relative magnetic permeability, ε_r is the relative permittivity, s is the electrical conductivity, and ω is the angular frequency.

It is expected that g has a wavelength dependence, but ρ_0 also has a wavelength dependence if the conductivity s is not negligible. Therefore after accounting for the wavelength dependence of g the residual dependence provides an estimate of s.

Since Mercury is similar in size to the moon and has a tenuous atmosphere, it is assumed that scattering directivity factor measured for the moon is also appropriate for Mercury. This g value should be a lower limit since the short pulse radar indicated that Mercury was rougher than the Moon. Evans and Pettengill [1963] derived the following expression for g:

$$g = (1 - x) + \frac{8}{3}x \tag{4}$$

where x represents the fraction of the surface radiating isotropically. For a wavelength of 68 cm, x was 8 percent, and for 3.6 cm, 14 percent, in the case of the Moon. Making a linear fit to these data $g(\lambda)$ is given as

$$g = 1.51 \times 10^{-1}\,(0.036 - \lambda\ (\text{meters})) + 1.234. \tag{5}$$

Assuming $\mu_r = 1$ in Equation (3), s is set to zero in Equation (3) for $\lambda = 3.8$ cm, and Equation (1) is solved for ε_r, using (2), (3), and (5). The resulting value of ε_r is 2.2, which is used to solve for s by iteration at $\lambda = 70$ cm. The resulting value of s is 2.1×10^{-2} (ohm meter)$^{-1}$. These values give a skin depth of 1/2 meter for the frequencies of interest.

These resulting values of ϵ_r and s can be taken as upper limits because $G(\lambda)$ was taken as a lower limit and, as in the case of the Moon, other loss mechanisms may be important. The actual conductivity value may be on the order of 10^{-6} (ohm meter)$^{-1}$.

REFERENCES

Evans, J. V., and G. H. Pettengill, The radar cross section of the Moon, J. Geophys. Res., 68, 5098, 1963.

Evans, J. V., and T. Hagfors, Radar Astronomy (McGraw-Hill, New York City, New York), 1968.

England, A. W., G. Simms, and D. Strangway, Electrical conductivity of the Moon, J. Geophys. Res., 73, 3219, 1968.

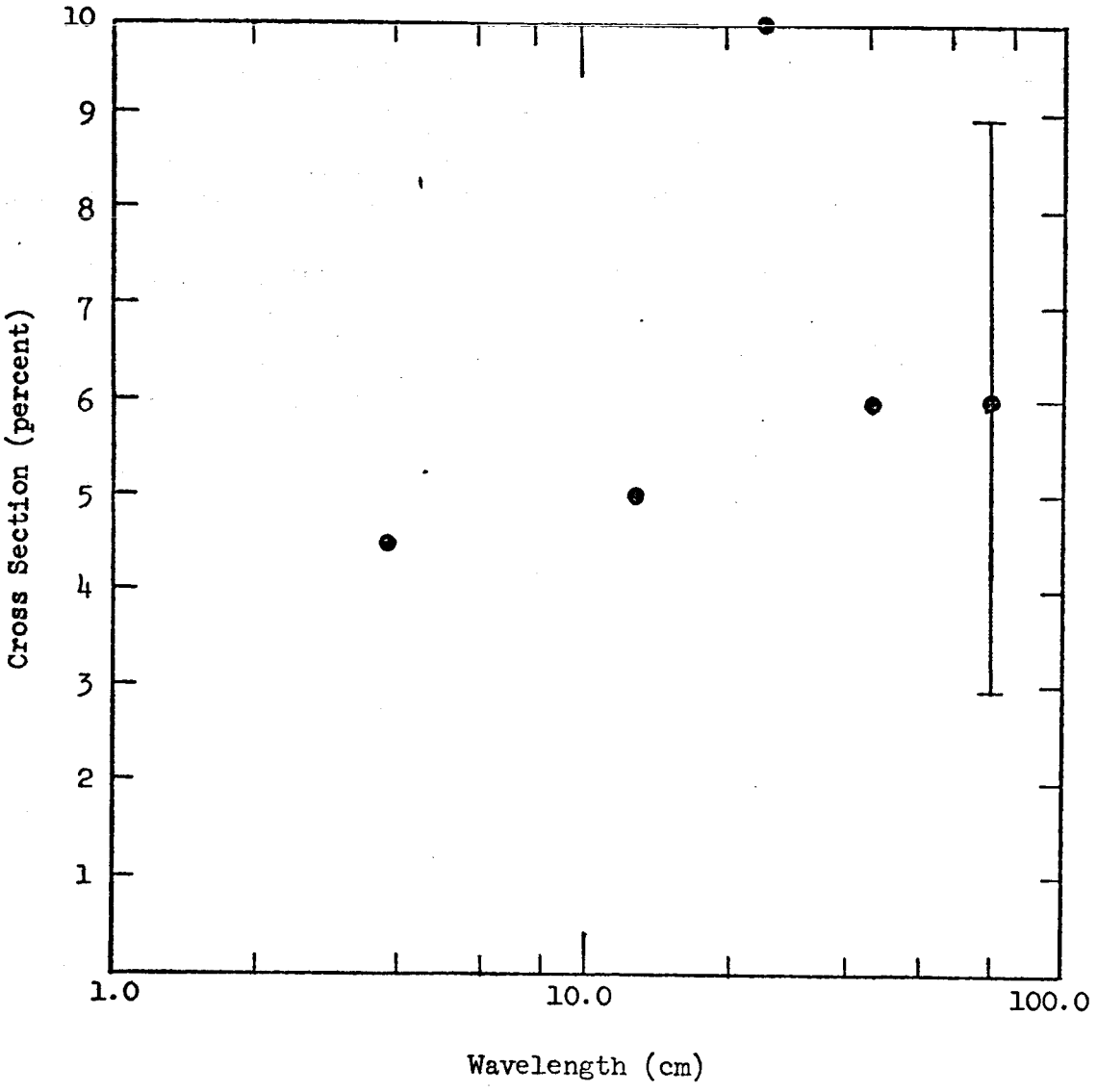

Figure 1.1 Radar Cross Section of Mercury

APPENDIX 2

ANOMALOUS RESISTIVITY IN A COLLISIONLESS PLASMA

When a dc electric field is impressed on a collisional plasma the electrons and positive ions are initially accelerated in opposite directions and the current begins to grow with time, but for $\nu t >> 1$ the many binary collisions produce enough scattering to limit the current. Ohm's law then applies and the conductivity is roughly given by $\sigma = Ne^2/m\nu$.

For a sufficiently dilute plasma, the number of binary collisions is negligible and one might tend to think of the system as a nearly perfect conductor. However, in any physical plasma, turbulence develops naturally when a dc electric field is applied, and this plasma turbulence produces scattering and finite resistivity.

One example of this is described in the left side of Figure A.2. Field and Fried (1964) performed a numerical experiment to obtain the current versus time profile for a nearly collisionless hydrogen plasma. When the relative drift becomes sufficiently high, the plasma becomes unstable with respect to the two-stream ion acoustic wave instability and waves grow rapidly, leading to the "anomalous" (and low) conductivity.

Whenever strong plasma turbulence develops, the effective scattering collision frequency is expected to be on the order of 10 percent of the maximum angular wave frequency (Coroniti, 1969). For ion acoustic waves we then have $\nu(\text{eff}) \simeq 0.1\ \omega_{p+}$ and when the Buneman modes are excited by bigger drifts, $\nu(\text{eff}) \simeq 0.1\ (m_-/m_+)^{1/3}\ \omega_{p-}$. Of course, these estimates are very qualitative, but there is some experimental verification of the numbers. The right hand side of Figure A.2 contains several points taken from laboratory experiments and this shows that when the field is too small to cause instability, the coulomb conductivity applies. However, as E is increased the system apparently generates ion sound waves, and then the Buneman modes, leading to further reductions in conductivity.

The shock observations discussed in Section II.3 also indicate that these concepts are roughly correct, and the semi-empirical relations cited on Figure A.2 were used to predict the solar wind conductivity near Mercury, as given in Figure II.3

REFERENCES

Field, E. C., and B. D. Fried, Solution of the kinetic equation for an unstable plasma in an electric field, Phys. Fluids, 7, 1937, 1964.

Coroniti, F. V., Electric field and currents, Planetary Electrodynamics Edited by S. C. Coroniti and J. Hughes (Gordon and Breach Science Publishers, New York), 359, 1969.

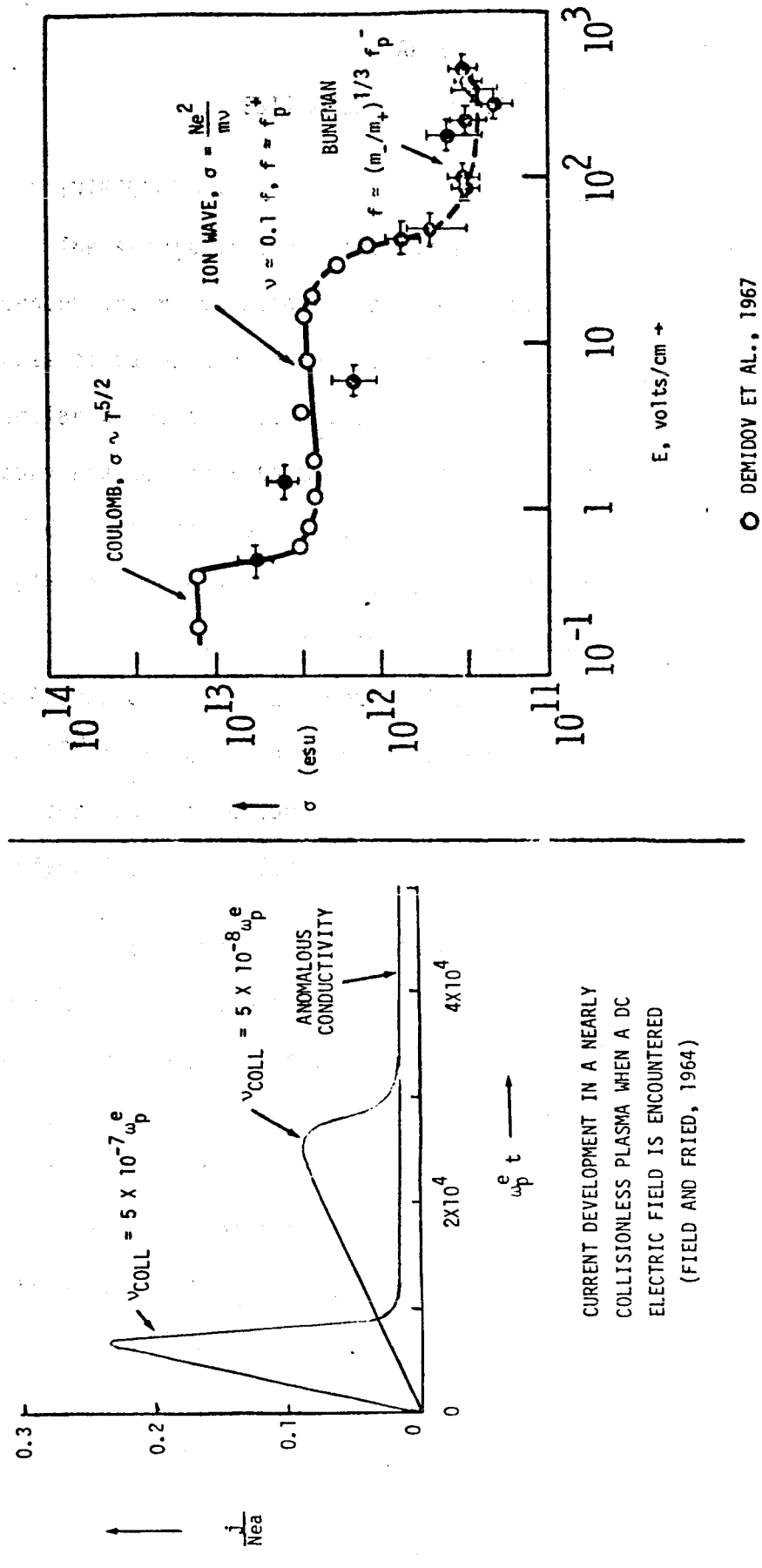

CURRENT DEVELOPMENT IN A NEARLY COLLISIONLESS PLASMA WHEN A DC ELECTRIC FIELD IS ENCOUNTERED (FIELD AND FRIED, 1964)

Figure 2.1

APPENDIX 3

ESTIMATES OF MERCURY'S ATMOSPHERE

I. INTRODUCTION

The spirit of these estimates is simply to demonstrate what could be happening under the rather loose restrictions on our calculations. The sources of gases considered herein are far from a complete set, but such molecular gases as H_2O, O_2, SO_2, etc. evolved by hypothetical vulcanism on Mercury are so far into the realm of wild speculation that they have been avoided. The ideas of accretion of gases during solar wind contact with the planetary surface are based only upon assuming that Ne and A^{36} are in the solar wind with approximately the abundances listed in Aller's book "The Abundance of the Elements" (Interscience, New York, 1961). The radiogenic A^{40} is calculated assuming a chondritic-like K^{40} content of 2.5×10^{-7} grams per gram of Mercurial stuff, at a branching ratio $\sim$ 10 percent, and a surface layer of effective depth 10 Km.

The loss mechanisms are standard. We first estimate the lifetimes of gravitationally bound species. The loss mechanism for this model is labeled "thermal escape only" in our density tables. For hydrogen at an equatorial temperature of 900°K assumed here, H is barely bound gravitationally, while for A^{36}, A^{40} and Ne^{20} the gravitational-thermal escape lifetimes are quite large. On the other hand, the scattering (scouring) of the atmospheric gases in the limb regions by solar wind protons is an obvious loss mechanism, whose computed lifetime for H is greater than that for thermal escape, while for A and Ne the scattering lifetime is very much less than the thermal escape time. The third loss mechanism is based upon assuming that every ion, formed

by combined photoionization and charge exchange with solar wind protons, is immediately lost by the atmosphere. Thus this model has a lifetime equal to the inverse ionization rate, and except for hydrogen, this lifetime is even shorter than the scattering lifetimes of A and Ne.

II. ASSUMPTIONS

Subsequent calculations are based on the following assumptions about conditions at Mercury:

1) We assume a noon surface temperature of 900°K. This value is perhaps higher than the value quoted by Rasool, Gross and McGovern (1966) of 616°K. Indeed, if the noon temperature were this low, hydrogen concentrations would exceed the values we have computed, unless we consider our temperature as that of the top of an atmosphere heated from above.

2) We have used the astronomical parameters for Mercury as listed in the American Handbook of Physics. These are $R = 0.38\ R_E$, $\rho_\oplus = 5.48$ gm-cm^{-3}, $V_e = 4.3$ km-sec^{-1}, $g_o = 372$ cm-sec^{-2}, solar radiation enhancement of 6 over earth, solar wind flux $\Phi_W = 2 \times 10^9$ protons-cm^{-2}=sec^{-1}.

3) K^{40} abundance in Mercury's crust 2.5×10^{-7} gm/gm, half-life $T_d = 1.3 \times 10^9$ yr $\approx 4 \times 10^{16}$ sec, distributed uniformly in 10 km thick layer.

4) Solar wind ions of all species striking the surface are assumed to neutralize and then evaporate at the surface temperature (900°K) in a lunar-like interaction.

5) Mercury has a negligible intrinsic magnetic field.

III. SOURCES OF GAS

We consider only solar wind accretion processes and the radiogenic A^{40} due to K^{40} decay in the crust. The only accreted gases considered are A^{36}, Ne^{20} and H. In Table I we show the thermal speeds, scale heights and gravitational binding lifetimes of the gases considered. Here $c_i^2 = 2\kappa T/m_i$, $h_i = c_i^2/2g_o$, and

$$\tau_i = \frac{2(6\pi)^{1/2} c_i^3}{9 g_o V_e} \exp\left(3V_e^2/2c_i^2\right) \qquad (1)$$

valid as long as V_e = escape speed exceeds c_i sufficiently.

Table I

gas	H	Ne	A^{36}	A^{40}
c_i(km-sec^{-1})	3.9	0.87	0.65	0.615
h_i(km)	4×10^3	200	113	100
τ_i(yr)	$\sim 10^{-4}$	$\sim 10^8$	$\sim 10^{20}$	$\sim 10^{21}$

The flux of the i^{th} solar wind constituent gas to Mercury's surface is

$$\Phi_{in} = A_i \Phi_W$$

$A_i = n_i/n$ = abundance of i^{th} species relative to hydrogen.

The thermal evaporation flux is just

$$\Phi_{evap} = \Phi_{in} = n_i(0) c_i$$

which yields a no-loss surface density of

$$n_i(0) = A_i \Phi_W / c_i \ . \tag{3}$$

However, if the lifetime of the i-th constituent is τ_i < age of planet, the expected surface density is simply

$$n_i(0) = A_i \Phi_W \tau_i / h_i \ . \tag{4}$$

The radiogenic A^{40} concentration is computed from the expression

$$n_i(0) = \frac{(\Delta R)(\rho_\theta)(2.5 \times 10^{-7})(0.1)(2^{\tau/T_d}-1)}{(W)(1.67 \times 10^{-24})\ h_i} \tag{5}$$

Where ΔR is the effective crustal layer containing K^{40}, τ_i is the lifetime for the loss mechanism assumed, T_d the half-life, W the number of nucleons (proton masses) the numerical factors being self-explanatory (present abundance of K^{40}, branching ratio, and proton mass in gm).

IV. LOSS MECHANISMS

a) The thermal evaporation against gravitational binding has a lifetime τ_i given by Equation (1) of the previous section, and Table I.

b) The scattering of atmospheric atoms by collisions with solar wind protons we estimate to be effective only on the limb, since knock-on collisions directed at the surface do not count. A rough consideration of the geometry leads to an estimate that about 1/6 of the atmosphere could be lost by such scattering. The lifetime against this loss mechanism is then

$$\tau_i \approx .6/\Phi_W \sigma_i \sim 3 \times 10^6 \text{sec}$$

if we use a solar wind flux of $2 \times 10^9 cm^{-2}\text{-}sec^{-1}$ and an elastic cross section $\sigma_i \approx 10^{-15} cm^2$.

c) If the loss of every atmospheric ion immediately upon formation is assumed, then the lifetime against total loss of all ions is just the inverse of the ionization rate. Ionization processes we restrict to photo-ionization and charge exchange with solar wind protons. If the photo-ionization cross section is σ_{ph}, that of charge exchange σ_{ex}, Φ_W the proton flux, and $\Phi(h\nu)$ the effective photon flux, then

$$\tau_i = (\sigma_{ph}\Phi(h\nu) + \sigma_{ex}\Phi_W)^{-1} \quad .$$

V. FRACTIONAL IONIZATION

The fractional ionization of the i^{th} species due to photons and charge exhange is readily shown to be

$$n_i^+/n_i = \xi_i = \frac{2}{\tau_i} \cdot \frac{c_i}{g_o} \quad .$$

In Table II we show values for the indicated gases

Table II

Gas	$\Phi(h\nu)$	σ_{ph}	σ_{ex}	τ_i(sec)	ξ_i
H	-	-	10^{-16}	5×10^6	2×10^{-4}
Ne	1×10^{11}	7×10^{-18}	5×10^{-16}	5.7×10^5	8×10^{-4}
A	1.6×10^{11}	2×10^{-17}	7×10^{-16}	2.2×10^5	8×10^{-4}
N	1.6×10^{11}	5×10^{-18}	5×10^{-16}	5.5×10^5	1×10^{-3}

VI. DENSITIES PREDICTED AT SURFACE

In Table III we give the number density of neutral gases at the planet surface in cm^{-3} for the indicated loss mechanisms. In Table IV we give the corresponding ion densities.

Table III

Ion	H	N_e	A^{36}	A^{40}	Total
Abundance/H	1	$5x10^{-4}$	$8x10^{-6}$	-	-
Thermal escape	$1.5x10^{4}$	$1.5x10^{14}$	$1.7x10^{14}$	$2.6x10^{15}$	$3x10^{15}$
Scattering [b]	$(1.5x10^{7})$[a]	$1.5x10^{5}$	$4.2x10^{3}$	$2x10^{4}$	$2x10^{5}$
Total loss all ions [b]	$(2.5x10^{7})$[a]	$2.9x10^{4}$	$3.1x10^{2}$	$1.5x10^{3}$	$4x10^{4}$

a: Limited to $\sim 10^{4}$ by thermal escape

b: $\Phi_W = 2 \times 10^{9}$ protons-cm^{-2}-sec^{-1} used

Table IV

Ion	H^+	N_e^+	A^{36+}	A^{40+}	Total
Thermal escape	3	$1.2x10^{11}$	$1.4x10^{11}$	$2x10^{12}$	$2.3x10^{12}$
Scattering [b]	3[d]	120	3	16	140
Total loss all ions [b]	3[a]	24	0.25	1.2	30

a: Limited by thermal escape

b: $\Phi_W = 2 \times 10^{9}$ protons-cm^{-2}-sec^{-1} used

VI DISCUSSION

According to the foregoing estimates, the atmospheres which are most likely (within the limits of our models) are those which are limited by either solar wind scattering or total escape of all ions. These atmospheres are tenuous and are dominated by Ne.

If we had considered the solar wind accretion of nitrogen, of relative abundance 10^{-4} per H^+, then its partial density would be 4×10^3 for total loss of all ions and 2×10^4 for the scattering loss model. The corresponding ion densities are 4 and 20, respectively. Thus, N could be competitive with A^{40} if the latter gas is present.

As a matter of fact, one must consider the possibility of a very low temperature on the dark side of Mercury. At 1 mm Hg vapor pressure, the freeze-out for A, Ne and H require that

A: $T_{MIN} < 54°K$

Ne: $T_{MIN} < 15°K$

H: $T_{MIN} < 10°K$

It is not clear just how much lower these temperatures become for the much lower vapor pressures indicated in Table III. However, it would appear that only argon is in danger of being pumped out of the atmosphere by the cryogenic action of the dark side surface.

This would leave H, Ne and perhaps nitrogen, all accretion products arising from solar wind bombardment of the surface. The heavy ion densities

in Table IV compete with the solar wind density ($\sim$ 30 cm^{-3} at 0.4 A.U.). Especially, if the ion density is as high as that predicted by the scattering loss model, even at one Ne scale height of 200 km (over the equator) one still has some 40 cm^{-3} of Ne^{+} at $\sim$ 900°K ($\sim$ 0.08 eV) mixed with a hot proton wind ($\sim$ 1 keV) of comparable density. Since the solar wind electron temperature is also high compared to 900°K, the plasma layer of some hundreds of km may contain micro-instabilities leading to a relatively high resistivity (low conductivity) in the layer. This would screen out inductive heating of the planet by magnetic field interactions quite effectively. It would also lead to some as yet undetermined effects on the wake-cavity boundary layer.

It seems very likely that any primitive atmosphere containing CO_2 would have been scoured away by solar wind scattering and ion escape. Any CO_2 present would have to have been generated within a scattering or ion escape lifetime by tectonic processes within the planet. However, a dark side temperature less than $\sim$ 150°K would freeze out this CO_2 quite effectively. Similar comments would apply to SO_2, O_2 and other volcanically generated gases.